NASA CONTRACTOR REPORT

NASA CR-1678

AN EXPERIMENTAL AND THEORETICAL INVESTIGATION OF PLANE-STRESS FRACTURE OF 2024-T351 ALUMINUM ALLOY

by C. E. Feddersen, F. A. Simonen, L. E. Hulbert, and W. S. Hyler

Prepared by
BATTELLE MEMORIAL INSTITUTE
Columbus, Ohio 43201
for Langley Research Center

NATIONAL AERONAUTICS AND SPACE ADMINISTRATION • WASHINGTON, D. C. • SEPTEMBER 1970

1. Report No.	2. Government Accession No.	3. Recipient's Catalog No.
NASA CR-1678 (call no)		

4. Title and Subtitle	5. Report Date
AN EXPERIMENTAL AND THEORETICAL INVESTIGATION OF PLANE-STRESS FRACTURE OF 2024-T351 ALUMINUM ALLOY	September 1970
	6. Performing Organization Code

7. Author(s)	8. Performing Organization Report No.
C. E. Feddersen, F. A. Simonen, L. E. Hulbert, and W. S. Hyler	None

9. Performing Organization Name and Address	10. Work Unit No.
Battelle Memorial Institute Columbus Laboratories 505 King Avenue Columbus, Ohio 43201	126-14-03-27-00
	11. Contract or Grant No. NAS1-8522
	13. Type of Report and Period Covered: Contractor Report
12. Sponsoring Agency Name and Address: National Aeronautics and Space Administration, Langley Research Center, Hampton, Virginia 23365	14. Sponsoring Agency Code

15. Supplementary Notes

16. Abstract

A theoretical and experimental study was conducted on the plane-stress fracture behavior of precracked 2024-T3 aluminum alloy sheet and plate (-T351) panels. The influence of width, thickness, and crack-aspect ratio on the residual strength of centrally cracked panels was determined. An engineering analysis was also performed on the data utilizing several analytical and empirical fracture expressions. A more generalized data display and analysis technique was discussed. A theoretical analyses of plastic zones included both the boundary-point-least-square method on the Dugdale model, and a two-dimensional analysis by the finite-element method. Photoelastic determinations of the plastic-zone size and shape were used for validation.

17. Key Words (Suggested by Author(s))	18. Distribution Statement
residual strength, fracture, aluminum alloy, plane stress, plasticity, fracture analysis methods, width effect.	Unclassified – Unlimited

19. Security Classif. (of this report)	20. Security Classif. (of this page)	21. No. of Pages	22. Price*
Unclassified	Unclassified	78	$3.00

*For sale by the Clearinghouse for Federal Scientific and Technical Information
Springfield, Virginia 22151

TABLE OF CONTENTS

TABLE OF CONTENTS
(Continued)

LIST OF SYMBOLS

a = Sum of half crack length and plastic zone size, $c + r$

C_m = Crack sensitivity

$2c$ = Crack length

$2c_o$ = Initial crack length

$2c_1$ = Crack length at onset of acceleration pulse at critical instability

$2c_2$ = Crack length at end of acceleration pulse at critical instability

E = Young's modulus

E_1 = Secant modulus at ultimate strength

G = Strain energy release rate

$2h$ = Length of rectangular plate

K = Stress intensity factor

k_w = Dixon's finite-width correction

R = Stress ratio

r = Length of plastic zone

S = Gross stress

S_o = Gross stress at onset of slow crack growth as determined by 5 percent secant offset

S_1 = Maximum gross stress

S_n = Net section stress

T = Thickness

TUS = Tensile ultimate strength

u, v = Components of displacement

v_c = Crack-tip displacement

v_o = Crack opening displacement

W = Plate width

x, y = Rectangular coordinates

Y, TYS = Yield stress

z = Complex variable $x + iy$

γ_{xy} = Shear strain

2δ = Deflection of plate

ϵ_x, ϵ_y = Strain components

ϵ_1, ϵ_2 = Principal strains

$\kappa = (3 - \nu)/(1 + \nu)$

μ = Modulus of elasticity in shear

ν = Poisson's ratio

ρ' = Neuber constant

σ_x, σ_y = Stress components

σ_1, σ_2 = Principal stresses

$\bar{\sigma}$ = Equivalent stress

τ_{xy} = Shear stress

ϕ = Complex stress function

ψ = Complex stress function

AN EXPERIMENTAL AND THEORETICAL INVESTIGATION OF PLANE-STRESS FRACTURE OF 2024-T351 ALUMINUM ALLOY

by

C. E. Feddersen, F. A. Simonen, L. E. Hulbert, and W. S. Hyler

SUMMARY

A theoretical and experimental study was conducted on the plane-stress fracture behavior of precracked 2024-T3 aluminum alloy sheet and plate (-T351) panels. The influence of width, thickness, and crack-aspect ratio on the residual strength of centrally cracked panels was determined. An engineering analysis was also performed on the data utilizing several analytical and empirical fracture expressions. A more generalized data display and analysis technique was discussed. A theoretical analyses of plastic zones included both the boundary-point-least-square method on the Dugdale model, and a two-dimensional analysis by the finite-element method. Photoelastic determinations of the plastic-zone size and shape were used for validation.

INTRODUCTION

As performance requirements on aerospace systems have been increased, design loadings and reliability requirements have also increased. Sophisticated structural analysis tools and modern design philosophies have contributed significantly to increasing structural efficiencies without sacrificing safety and reliability. However, further advancement of the technology now requires more definitive assessment of the damage susceptibility and damage tolerance of the materials from which the structure is made.

The primary emphasis in damage tolerance studies in the past decade has been directed toward relatively high-strength materials which exhibit relatively "brittle" failures. In this program, the study was directed toward a more ductile material, 2024-T3 aluminum alloy, emphasizing the very specific facet of plane-stress fracture. The program was considered in three parts: (1) experimental studies, (2) engineering evaluation, and (3) theoretical analysis. The experimental studies were conducted in two phases to delineate thickness and width effects in the 2024-T3 aluminum alloy. Engineering evaluations were conducted on these and other data by a variety of techniques to ascertain the practical significance of the data and the methods. Throughout the program, theoretical correlations were made to relate the experimental results with advanced techniques of plastic-zone modeling. These tasks and their results are presented in the following report.

EXPERIMENTAL STUDIES

Introduction

To fulfill the experimental objectives of this program, it was necessary to conduct an initial control exploratory study prior to the final selection of specimen thicknesses and widths. In order to correlate with previously generated NASA fatigue and fracture data, it was decided to use an 8-inch-wide specimen as the initial baseline for thickness studies. A single crack-aspect ratio, $2c_o/W$, of one-third was used in these tests. The data derived from this portion of the program are presented and analyzed in Appendix A. A thickness effect was apparent; but it was not large for this specimen width.

As a result of these preliminary studies, three sheet or plate thicknesses, 0.05-, 1/8- and 1/2-inch, were selected for the main plane-stress study. As part of the main program, the additional variables of panel width and crack aspect ratio were included. To consider a distinctly larger width and, yet not exceed dimensions of practical interest, a 24-inch panel width was chosen. In the control tests, it had become apparent that, for the 2024-T3 material, nominal net section yielding or tensile instability was the nominal failure criterion for 8-inch-wide panels. The selection of lesser width would only re-emphasize that fact. However, to physically confirm that conjecture, a set of 4-inch-wide specimens of the median-thickness, i.e., 1/8 inch, was included. Among these combinations of thickness and width, the additional variable of initial crack aspect ratio, $2c_o/W$, was included. Three values, 0.1, 0.3, and 0.6, were used. The resultant array of crack lengths used was:

	Crack Aspect Ratio			
Width	0.1	0.3	0.6	Thicknesses
4	0.4	1.2	2.4	1/8
8	0.8	2.4	4.8	0.050, 1/8, 1/2
24	2.4	7.2	14.4	0.050, 1/8, 1/2

In subsequent sections, the details of specimen preparation and fracture test procedures are discussed. In support of the theoretical studies, a photoelastic analysis included a confirmation of the plastic-zone model predicted by the finite-element analysis. These details are also presented. Finally, the experimental data are presented in tabular and graphical displays.

Practical Aspects

To provide the basis for the discussion of test techniques and data collection and reduction, this section contains a discussion of certain practical features associated with the rising-load fracture test.

Consider the load-flaw size relationship illustrated in Figure 1. As an initial loading is applied to a flawed element, no change in flaw size is noted. This is reflected as a vertical line in the figure. However, as this load rises above a given level, some flaw growth is observed. This load or stress level is termed the threshold of slow flaw growth. With increasing load the flaw size also increases, producing the frequently ragged and irregular slow-growth path indicated in the figure. The character of this path is dependent on the sensitivity of instrumentation, type of strain control (load rate or stroke rate), and material properties. This slow-growth mode continues in a generally monotonic fashion until a critical flaw size is reached where fracture occurs. Here the flaw penetrates the cross section and the structural load is dissipated.

An exact determination of threshold and critical flaw conditions is very elusive. However, several practical techniques for estimating, or at least bracketing these conditions, are available. First consider the threshold of flaw growth. During the rising-load test, the specimen response is recorded as a typical load-deflection curve, as illustrated in Figure 2. The deflection may be the crack opening displacement (COD) or the deformation measured over some specified gage length. During the initial stage of loading the load-deflection curve is linear as would be expected from elastic mechanics theory. At some point of loading, detectable nonlinearities will become apparent and may be attributed to plastic deformation, crack growth or a combination of the two. Experience in thick-section (plane-strain) fracture testing has shown that under certain specified conditions, the 5 percent secant offset intercept on a load-deflection record is a reasonable estimate of the onset of slow growth. [1]* While the conditions of plane stress are substantially different, this offset technique is a consistent and convenient means of marking the threshold of nonlinear specimen behavior which, from a design perspective, is quite important. In this program, the threshold of crack growth was identified both visually and mechanically. The visual determination is somewhat arbitrary in that shadows at the crack tip due to plastic straining obscure crack movement. Furthermore, it is well known that varying degrees of internal crack growth (or tunneling) occur, thus making such surface observations only an "estimate" of the threshold of cracking. As a complementary measure of the onset of slow growth, from the corresponding load-compliance record, the 5 percent secant-offset stress, S_o, was determined graphically. While the correlation was fairly good, the latter values were utilized in the data analysis because of their simplicity and reproducibility in mechanical-testing procedures.

Now consider the critical flaw conditions interfacing between slow, stable tear and rapid, unstable crack propagation as illustrated in Figure 3. As the critical fracture condition is approached in the last stage of slow crack growth, the explicit designation of a single, unique critical crack length is very difficult because of the acceleration zone. In this program, to converge on or bracket this critical area, two final crack lengths, $2c_1$ and $2c_2$, were identified. From plots of crack length versus movie frames, the shorter crack length, $2c_1$, was selected as the deviation from linearity where the crack growth appeared to accelerate. In a similar fashion, the longer crack length, $2c_2$, was selected at the subsequent linear tangency where the crack appeared to be moving at a high, but constant (no further acceleration) velocity. Although these crack lengths are arbitrary in their determination, they bracket the critical-acceleration phase of rapid crack propagation. Because the time differential (approximately/sec) associated with this crack motion was so short, significant deviation from the maximum load, or stress, S_1, could not be discerned.

* Numbers in parentheses indicate reference numbers in List of References.

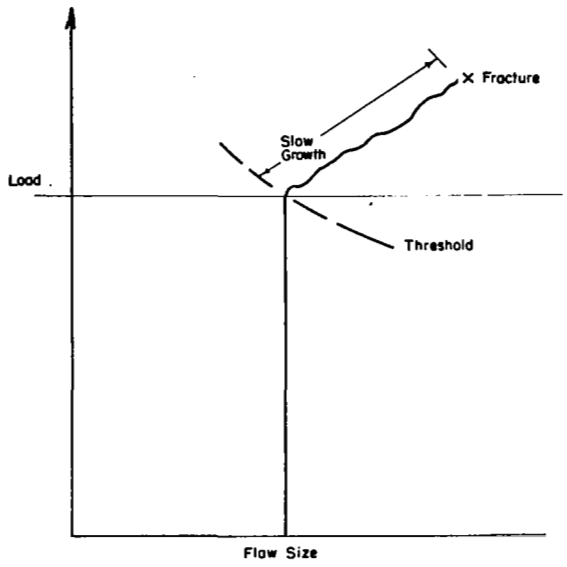

FIGURE 1. TYPICAL LOAD-FLAW SIZE RELATIONSHIP IN THE RISING-LOAD TEST

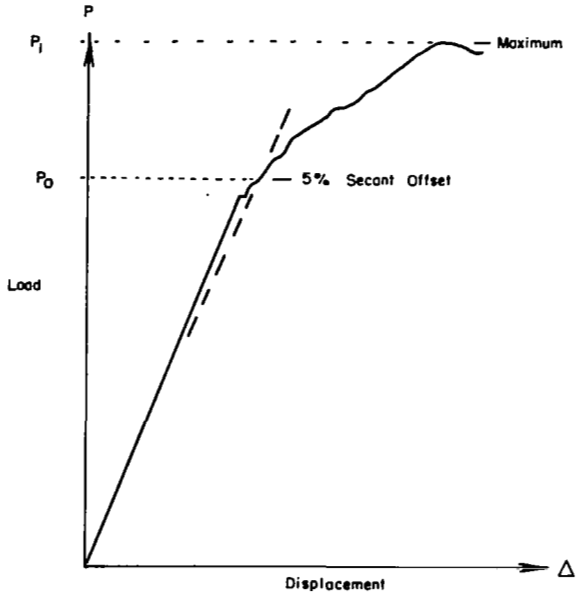

FIGURE 2. TYPICAL LOAD-DEFLECTION RECORD

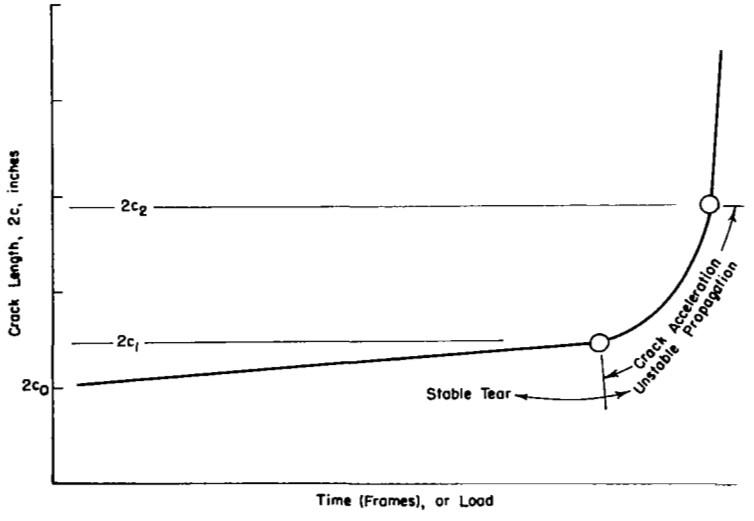

FIGURE 3. TYPICAL SLOW-GROWTH RECORD

Specimen Preparation

Material

All specimens were machined from bare 2024-T3 or T351 sheet or plate. Duplicate tensile tests were conducted to verify typical mechanical properties for each material. The data are listed in Table 1. Tensile properties and microstructures of the materials were found to be typical of this alloy and heat treatment.

TABLE 1. VERIFICATION-TEST DATA FOR TENSILE PROPERTIES OF 2024-T3 ALUMINUM ALLOY FOR THE MAIN PROGRAM

Specimen	Thickness, inch	0.2 Percent Yield Strength, psi	Ultimate Tensile Strength, psi	Elongation, percent in 2 inches
1	0.049	52,400	71,500	20.0
2	0.049	52,900	71,500	19.0
Average		52,650	71,500	19.5
1	0.123	53,700	71,500	20.0
2	0.123	53,900	71,800	20.0
Average		53,800	71,650	20.0
1	0.508	54,900	71,400	22.5
2	0.508	54,800	71,300	23.0
Average		54,850	71,350	22.7

Specimen Configuration

Figure 4 shows the essential details of fracture specimens used in the main program.

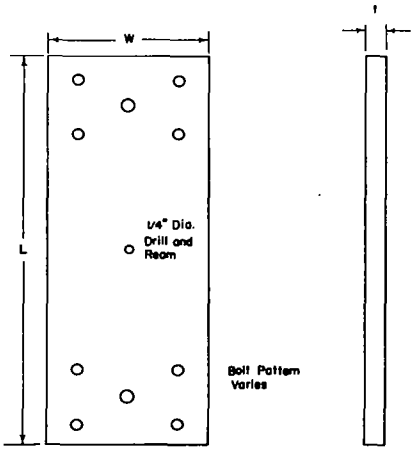

FIGURE 4. SPECIMEN CONFIGURATION FOR 4-, 8-, AND 24-INCH-WIDE SPECIMENS

Specimen Precracking

Following machining of the specimens, a saw cut perpendicular to the specimen surface and perpendicular to the loading direction was made to a total length equal to 0.8 inch less than the desired initial crack length for the fracture test. The last 0.8 inch (0.4 inch on each side) of the initial flaw was produced by fatigue cycling the specimen at a stress ratio R = 0.1 at stress levels as discussed below.

To eliminate stopping the test to measure crack length during fatigue cracking, a Strobo-slave was integrated into the electronic circuit so that it was triggered at the peak load of each cycle. By triggering at peak load, the crack movement was "frozen" at a time of maximum crack opening. In this manner, accurate measurements of crack length were obtained.

The actual crack-length measurements were performed optically. A transparent plastic sheet with an embossed grid of 1/10-inch spacing, prepared photographically, was centered on the EDM flaw. A 32X short-distance viewing telescope was used to monitor the crack length.

Broek and Schijve have shown that, for tests at R = 0.1, a propagating fatigue crack in 2024-T3 will change from a flat to a 45-degree slant made at a stress-intensity factor K = 21.5 ksi $\sqrt{\text{in.}}$ [3] Therefore, all fatigue cracking was accomplished at stress levels that would result in a final stress-intensity factor less than 20 ksi $\sqrt{\text{in.}}$ when the crack reached the desired length. When necessary (large 2c/W ratios, or on thin material), 1/4-inch-thick steel plate buckling guides lined with wax paper were used to prevent buckling during precracking. This procedure resulted in a flat final crack with essentially straight crack fronts for all conditions studied.

Fracture Test Procedures

All specimens were fracture tested under load control in a 25 kip, 50 kip, 170 kip, or 700 kip load capacity electrohydraulic testing machines; the machine capacity was determined by the specimen thickness. The tests were conducted under load control at a loading rate that produced a strain rate of 0.005 in./in./min in the elastic-portion of deformation. The use of load control was selected to prevent an abrupt load drop-off when pop-in occurred since such a drop in load would not be anticipated in a service condition.

Buckling restraint was used in the program. The buckling guides used consisted of 1/4-inch-thick steel plates lined with waxed paper on the face contacting the specimens. A hole was drilled in one of the buckling guides to allow the insertion of the compliance gage. The other buckling guide possessed a 1/2-inch-wide slot machined along its width parallel with the crack plane to permit viewing the progress of the crack during the course of the test.

Motion pictures were taken at a camera speed of 200 frames per second. The photographic record was made of the entire test. During the test, an electric pulse about every 3 seconds triggered a light flash in the high-speed camera that made a short exposure on the side track of the film. The electric pulse also produced a blip

on a load-time graph that was being recorded. Thus the load on the specimen could be correlated with specific frames of the high-speed movie and an accurate record of crack length versus load determined during the slow-crack-growth period of each test.

Also, in the main program, where a photoelastic coating was applied to one half of one surface of the specimen, a 1/2-inch-thick plexiglass sheet was used to replace the buckling guide on that side of the specimen. This allowed color motion pictures to be made of the strain pattern throughout the entire test while still restraining buckling of the specimen at the crack. During these tests a high-speed camera was also used on the opposite side of the specimen to measure crack propagation, and side-track-marking lights in both cameras were triggered by the marking pulse described previously.

In addition to the motion-picture data, a double-cantilever-clip compliance gage was inserted in the drilled and reamed 1/4-inch-diameter hole at the center of the crack. This gage provided a record of the crack opening displacement (COD) during the fracture tests. The gage was constructed from 17-7 PH stainless steel and possessed a bridge of four active strain gages.

The compliance gage output was the X-axis input to an X-Y recorder, and the Y-axis recorded the load level. Calibration curves were constructed to give bridge output as a function of gage displacement.

The test setup for a typical fracture test with a photoelastic coating is shown in Figure 5. Thus, the record of each test consisted of a load-COD plot, a high-speed motion picture of the crack growth and, in some cases, a color movie of the strain distribution and the actual fracture surface. The analysis techniques that were examined using this data are presented in the following sections.

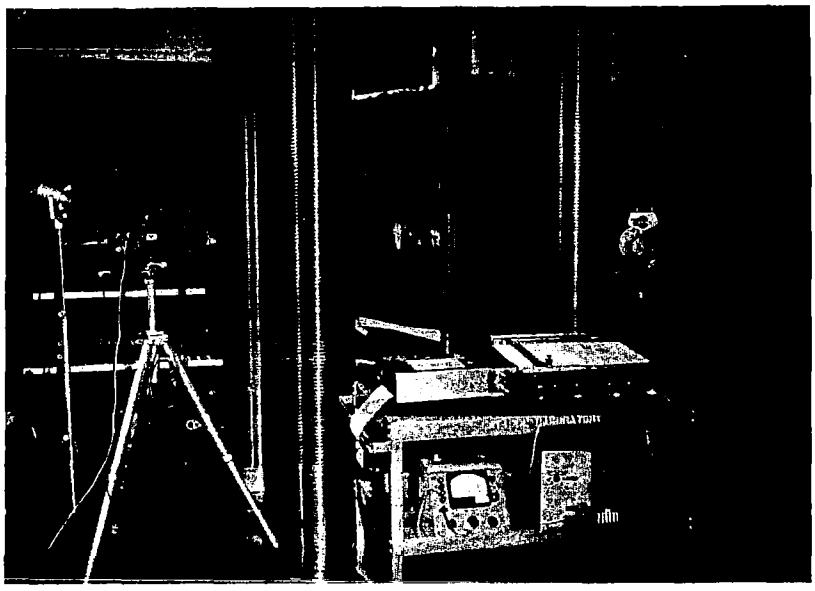

FIGURE 5. TEST EQUIPMENT USED FOR FRACTURE TESTS OF 24-INCH-WIDE 2024-T51 ALUMINUM ALLOY PANELS

Experimental Results

The experimental data generated in this program are presented in the following subsections.

Data Tables

The basic fracture data derived in this program are presented in Tables 2 through 4. The data format is quite straightforward. Following the specimen number column are the thickness and width columns denoting the measured gross dimensions of the critical section of the respective specimens. The next two columns are flaw size and stress values associated with the threshold or onset of flaw propagation. The initial crack length, $2c_o$ denotes the initial fatigue crack length existing prior to the rising-load fracture test. The five percent secant offset load stress derived from the load record was selected as the threshold stress, as discussed earlier. The final three data columns are associated with maximum load conditions. As discussed in an earlier section of this report, the 2024-T351 aluminum alloy appears to be characterized by a smooth slow-crack-growth process. As a result, two significant "final" crack length dimensions, $2c_1$ and $2c_2$, can be associated with maximum load and are separately tabulated. While the time increment in terms of motion-picture frames appears measurable, it is negligibly small in comparison with the loading rate. Thus, a single maximum-load stress, S_1, is noted with those crack lengths.

Graphical Displays

These fracture data are more vividly illustrated in Figures 6 through 11. Gross section stress is plotted versus crack length for each combination of thickness and width. Note that the data derived from each specimen are indicated by a connected trio of symbols. The lowest symbol of the trio represent the threshold conditions, or stress-flaw size combination, $(S_o, 2c_o)$. Of the upper points, the left-most denotes $(S_1, 2c_1)$ and the righthand point indicates $(S_1, 2c_2)$. Thus, this representation provides a semi-quantitative illustration of slow growth and fracture behavior. It is "semiquantitative" in the sense that more experimental work and criteria definition are required to specify this behavior adequately.

Initial Observations

From the data plots in Figures 6 through 11 two significant points are to be noted. One is that the critical fracture condition, as bracketed by the coordinate points $(2c_1, S_1)$ and $(2c_2, S_1)$, *essentially corresponds to a net-section yield criterion.* The other point is that the condition for threshold of flaw growth, i.e., the locus of points $(2c_o, S_o)$, is well below the net-section yield condition. That is, onset of slow growth appears to be an elastic process in the gross sense, while rapid fracture is characterized by tensile instability.

Some effect of thickness can be noted although it is only slight. The maximum fracture condition appears to decrease very slightly with increasing thickness. The only obvious width effect is a slight stretching of the crack acceleration segment $2c_1$-$2c_2$.

TABLE 2. FRACTURE DATA FOR 50-MIL-THICK 2024-T3 ALUMINUM ALLOY SHEET

Specimen	Thickness, T, in.	Width, W, in.	Initial Crack, $2c_0$, in.	5 Percent Secant Offset Stress, S_0, ksi	Final Crack Length, in. $2c_1$	Final Crack Length, in. $2c_2$	Maximum Stress, S_1, ksi	Remarks
99	0.051	8.0	2.66	19.1	2.8	3.6	31.3	Photoelastic test
102	0.049	8.0	4.77	17.1	4.9	5.75	19.2	
121	0.049	24.0	7.0	20.0	7.95	13.50	27.6	Photoelastic test
122	0.049	24.0	7.16	--	8.15	11.0	28.3	With buckling guides
123	0.049	24.0	14.27	12.3	15.0	18.0	16.5	
124	0.049	24.0	2.32	22.1	3.0	7.4	42.2	

TABLE 3. FRACTURE DATA FOR 1/8-INCH-THICK 2024-T3 ALUMINUM ALLOY SHEET

Specimen	Thickness, T, in.	Width, W, in.	Initial Crack, $2c_0$, in.	5 Percent Secant Offset Stress, S_0, ksi	Final Crack Length, in. $2c_1$	Final Crack Length, in. $2c_2$	Maximum Stress S_1, ksi	Remarks
111	0.123	4.0	2.4	--	--	--	44.9	Failed in grip
112	0.122	4.0	2.39	14.0	2.4	3.1	20.3	
113	0.123	4.0	0.39	32.1	0.5	1.0	46.0	
114	0.123	4.0	1.19	25.4	1.2	1.8	35.2	
115	0.123	4.0	2.34	15.2	2.4	2.9	20.5	
116	0.123	4.0	1.20	23.9	1.2	1.9	36.6	
97	0.124	8.01	2.6	21.0	2.75	3.30	34.3	Photoelastic test
103	0.123	8.00	0.8	18.3	0.85	1.90	46.4	
104	0.123	8.00	0.8	--	0.80	2.00	46.4	
105	0.123	8.00	4.7	12.7	4.70	4.90	20.5	With buckling guides
106	0.123	8.00	4.74	14.0	4.74	5.26	19.6	
125	0.123	24.0	7.2	--	8.4	11.8	28.0	With buckling guides
126	0.123	24.0	2.4	22.4	2.84	3.25	44.6	Photoelastic test
127	0.123	24.0	2.4	22.4	2.90	4.40	44.1	
128	0.123	24.0	7.15	13.6	8.6	11.6	29.2	
129	0.123	24.0	14.39	--	15.4	17.8	13.1	
130	0.123	24.0	14.35	7.8	14.4	16.2	15.4	

TABLE 4. FRACTURE DATA FOR 1/2-INCH-THICK 2024-T3 ALUMINUM ALLOY PLATE

Specimen	Thickness, T, in.	Width, W, in.	Initial Crack, $2c_0$, in.	5 Percent Secant Offset Stress, S_0, ksi	Final Crack Length, in. $2c_1$	Final Crack Length, in. $2c_2$	Maximum Stress S_1, ksi	Remarks
98	0.50	8.0	2.6	21.0	2.77	3.40	30.6	Photoelastic test
107	0.509	8.05	4.85	13.66	4.90	5.20	18.0	With buckling guides
108	0.509	7.96	4.82	12.83	4.80	5.00	18.0	
131	0.509	24.0	7.25	17.2	8.65	12.0	26.8	With buckling guides
132	0.509	24.15	7.20	18.55	8.0	11.5	27.6	
133	0.509	24.15	14.1	--	15.0	17.4	15.5	
134	0.509	24.15	2.30	25.7	2.8	4.8	42.8	

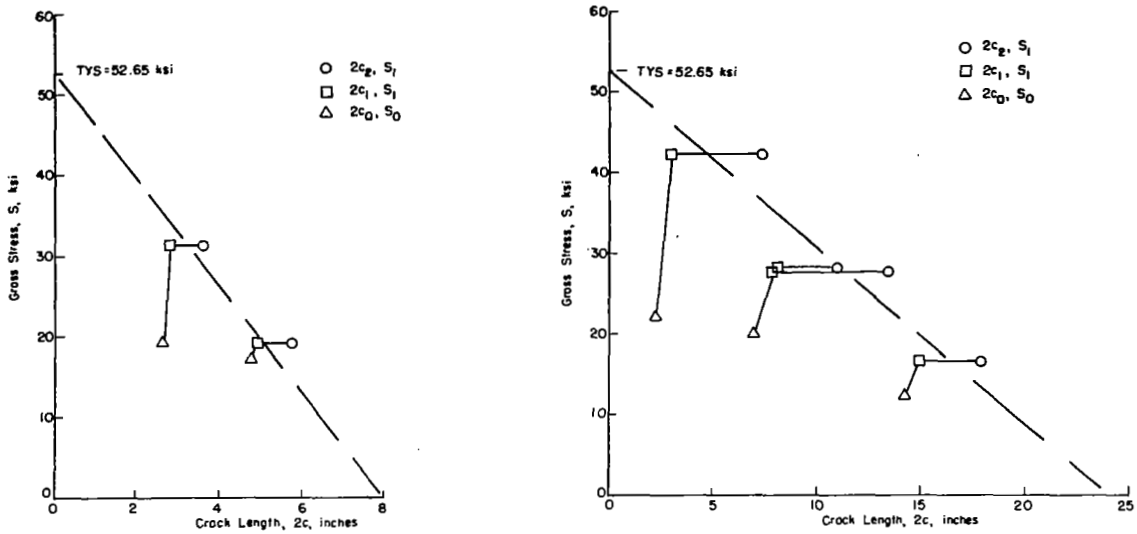

(a) 8-Inch-Wide Panels

(b) 24-Inch-Wide Panels

FIGURE 6. FRACTURE DATA FOR 50-MIL-THICK 2024-T3 ALUMINUM ALLOY SHEET

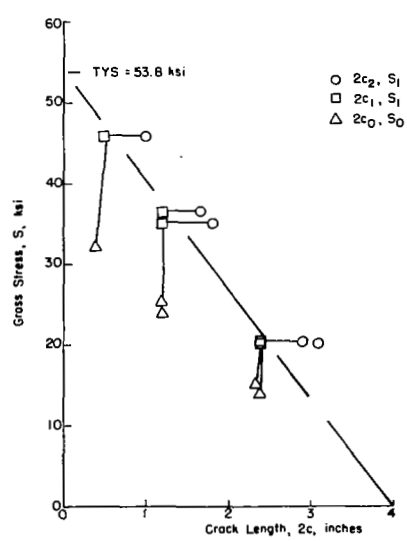

FIGURE 7. FRACTURE DATA FOR 1/8-INCH-THICK, 4-INCH-WIDE 2024-T3 ALUMINUM ALLOY SHEET

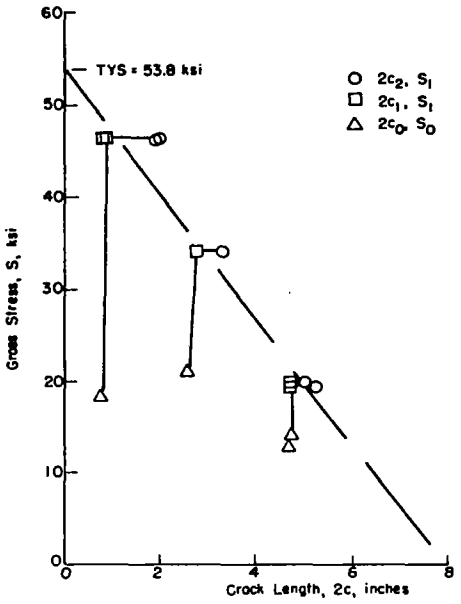

FIGURE 8. FRACTURE DATA FOR 1/8-INCH-THICK, 8-INCH-WIDE 2024-T3 ALUMINUM ALLOY SHEET

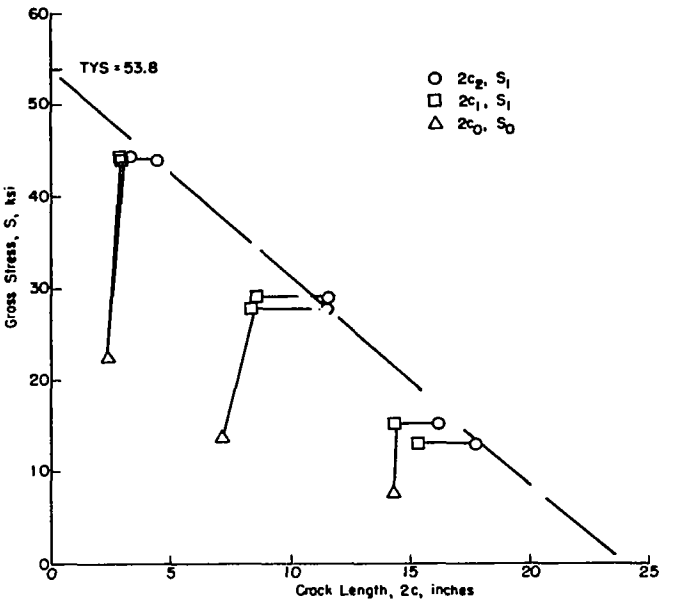

FIGURE 9. FRACTURE DATA FOR 1/8-INCH-THICK, 24-INCH-WIDE 2024-T3 ALUMINUM ALLOY SHEET

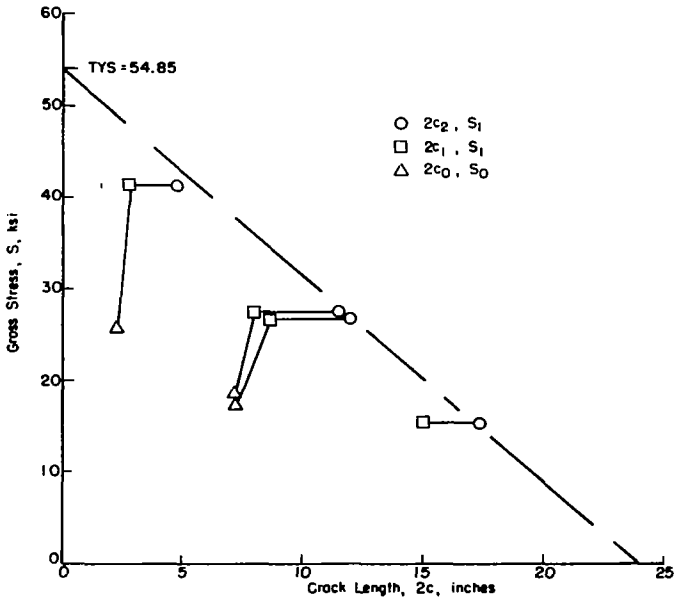

FIGURE 10. FRACTURE DATA FOR 1/2-INCH-THICK, 8-INCH-WIDE 2024-T351 ALUMINUM ALLOY PLATE

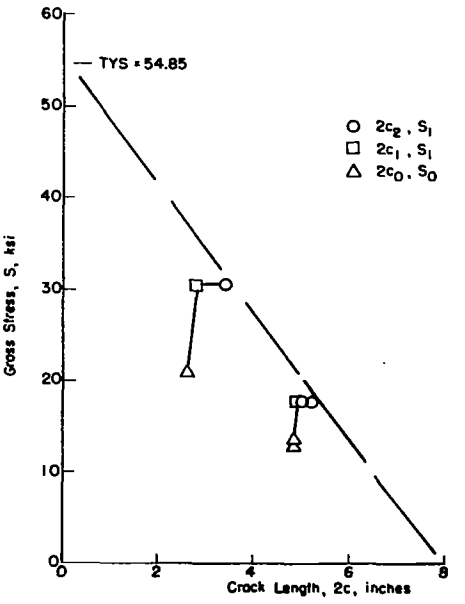

FIGURE 11. FRACTURE DATA FOR 1/2-INCH-THICK, 24-INCH-WIDE 2024-T351 ALUMINUM ALLOY PLATE

ENGINEERING EVALUATION

To be useful in practical applications, measures of material toughness (and their associated fracture characterization techniques) must serve two purposes. In addition to providing a comparative rating of materials, the toughness measure must also be easily relatable to the geometric and loading terms of structural design. In fact, this duality in the nature and the function of a toughness measure is a basic criterion for a truly useful fracture characterization technique.

In this portion of the report an overview of engineering fracture analysis is presented. First the general concepts of fracture toughness and residual strength are mentioned. Then, a general discussion of the principal fracture analysis methods is presented to appraise, interpret, and compare engineering techniques of fracture analysis and to selectively apply these data from other sources.

Fracture Toughness and Residual Strength

In the following discussion toughness, or fracture toughness is viewed as a material characteristic, and residual strength refers to the structural strength as influenced by fracture toughness, geometry, loading and so forth. This not-always-so-obvious distinction is very important to recognize. Of course, at this point in the discussion, this distinction is only conceptual; the purpose of the program is an elucidation of this concept. The goal in appraising fracture toughness is to obtain a quantitative description of the material itself. Then, in residual-strength studies, fracture toughness is applied to design situations.

In the most fundamental sense, the basic objective of toughness-testing and residual-strength studies is to determine the relationship between gross applied stress, S, (or load) and flaw size, 2c. For flat, centrally cracked tensions panels, these quantities (within their geometric framework) are graphically idealized in Figure 12. In this illustration, the constraint of finite size immediately suggests width as a basic parameter in the studies. Furthermore, the recognition of stress states (i.e., plane stress or plane strain) makes third-dimensional restraint, or "thickness effects" quite important. From here one can readily suggest additional parameters of temperature, environment, strain rate, etc.; however, these are beyond the scope of the current program. Since, in this program, the fracture behavior and toughness of flat, centrally cracked tension aluminum panels was studied, the following discussion emphasizes that geometric model. However, parallel discussions, observations, and arguments can be generated readily for other structural configurations.

Fracture Analysis Methods

The goal of fracture data analysis is the translation of experimental test results into meaningful and useful material and/or structural parameters. A variety of techniques, both theoretical and empirical, have been developed to describe various aspects of fracture in stress-related terms. These may be grouped into the following three major categories:

Stress-intensity factors

Effective-width techniques

Notch analysis or crack sensitivity.

These are discussed and compared in the following subsections. While not all are universally accepted, each has offered some insight to a particular problem and has been of value to some investigator. Within the following subsections the principal fracture models are briefly discussed and interrelated. The objective is to demonstrate the central coherent theme common to these models and to discuss their relative correlation. Finally a generalized method is discussed. The data-analysis phase of the fracture program includes an analysis of the data by selected techniques.

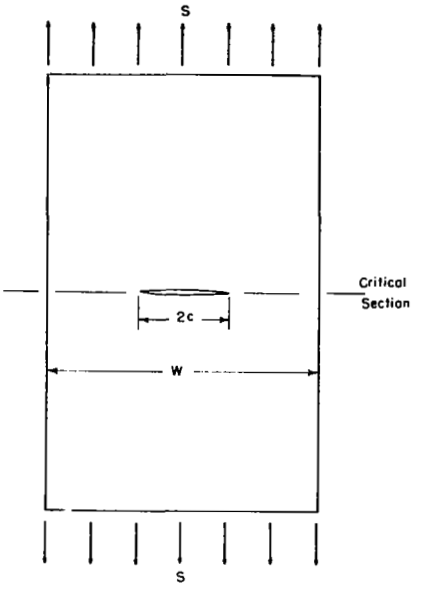

FIGURE 12. FLAT, CENTER-CRACKED TENSION PANEL

Stress-Intensity Factors

The Griffith-Irwin concept of brittle fracture is the foundation of linear-elastic-fracture mechanics.[4] It is based on the concept of a strain energy-release rate, G,

$$G = \frac{S^2 \pi c}{E} \quad , \tag{1}$$

or, equivalently, a stress-intensity factor, K,[5, 6, 7]

$$K = S \sqrt{\pi c} \tag{2}$$

for a center-cracked tension panel. This latter relation, while potentially very useful, is based on certain idealized conditions which are very difficult to duplicate in finite-size structural elements and imperfectly elastic (or real) materials. As a result, practical structural experiments are influenced by the following effects.

Width Effect. The development of Expression 2 is based on the idealization of a crack or flaw in a panel of infinite extent. Of course, in real engineering structures such a structural size is only hypothetical. A correction factor is needed to correlate fracture data obtained on finite-size elements and relate it to the reference baseline of an infinite-sized panel. To account for the effects of finite width, a factor, termed the finite-width correction, f(2c/W), has been used to modify the previous expression as

$$K = S\sqrt{\pi c}\ f(2c/W) \tag{3}$$

where

2c = crack length
W = panel width.

The finite width correction is in excess of unity, i.e.,

$$f(2c/W) \geq 1.0 \quad , \tag{4}$$

since the finite boundary tends to intensify the distribution of stresses in the area of the discontinuity. This is a more severe situation than for the equivalent flaw in an infinite-width panel. Alternatively, the finite-width panel may be viewed as having less section remaining to carry the cut-load and, hence, is being more severely loaded.

Thickness Effect. The effect of thickness is a bit more nebulous in its definition. The bulk restraint of thickness adjacent to the crack tip introduces a triaxial stress field which, in turn, tends to restrain plastic deformation. The extremes of thickness (i.e., plane stress, in reality a two-dimensional case where t = 0; and plane strain, t = ∞) are relatively easy to model analytically, but are only the extreme bounds to myriad real, finite-thickness cases. While an evaluation of the thickness effect was one objective of this program, it was essentially an empirical study. Intimately tied to this parameter is the effect of plasticity.

Plasticity Effect. From an analytical perspective, plasticity can be considered either as an effective extension of the crack length, or as an artificial amplification of the applied gross stress. In either case it tends to manifest itself as a relative increase in material toughness. Frequently, the influence of plasticity is appended to the crack length term of Expressions 2 and 3 as a plastic-zone radius, r, with the formulation,

$$K = S\sqrt{\pi(c + r)}\ f[\,2(c + r)/W] \tag{5}$$

Several analytical formulations of plastic-zone sizes have been postulated. Irwin presented the relations

$$r = \frac{1}{2\pi}\left(\frac{K}{TYS}\right)^2 \tag{6}$$

for plane stress, and

$$r = \frac{1}{4\sqrt{2\pi}} \left(\frac{K}{TYS}\right)^2 \approx \frac{1}{6\pi} \left(\frac{K}{TYS}\right)^2 \qquad (7)$$

for plane strain. With these expressions the computation is iterative on K. In contrast, Dugdale derived

$$r = c \left(\sec \frac{\pi}{2} \frac{S}{TYS} - 1\right) \qquad (8)$$

which for small values of S/TYS is equivalent to Expression (6) but at large S/TYS values is significantly larger.

Significance. The objective of characterizing a structural material in terms of a stress-intensity factor, K, is to determine a unique index of material crack resistance. This index could then be used in an inverse analytical procedure to predict critical fracture conditions. However, difficulties in test techniques and their standardization, unknowns in the above discussed parametric influences, and inherent material variables contribute to significant variance and scatter in the resultant data evaluation.

Effective Width Techniques

Briefly stated, the effective width techniques are concerned with the definition of a pseudo yield, or plastic zone over which the load cut by the flaw is redistributed. Two prominent techniques are described in the following subsections. In essence, they are intuitively motivated methods of designating a stress-flaw size curve for specific specimen data.

Due to Crichlow[8]. This engineering analysis of center-cracked tension panels assumes that the cut load in the panel is carried in the reserve strength of the panel immediately adjacent to the crack, as shown in Figure 13. This concept resolves to the expression,

$$S_{cr} = \frac{TUS}{1 + \frac{c}{W_e}} , \qquad (9)$$

or, when finite-width effects and experimental parameters are introduced,

$$S_{cr} = \frac{TUS}{1 + \frac{c}{W_o \tanh \left(\frac{B - 2c}{W_1}\right)}} , \qquad (10)$$

where

$$W_e = W_o \tanh \left(\frac{B - 2c}{W_1}\right)$$

B = specimen width

W_o, W_1 = empirical constants

This technique has been used extensively for modeling airframe structures and has been extended to include a variety of stiffening arrangements. Its fracture relation is a two-parameter expression which, while similar in function, has no ostensible relation to stress-intensity-factor concepts.

Due to Christensen and Denke[9]. As a variation on the effective-width theme, this method recognizes the Westergaard distribution of the stress, S, adjacent to the crack-tip. The summation of the idealized elastic stress, over a segment, W_e, is equated to a uniformly stressed plastic zone (at TUS) of the same dimension, W_e, as shown in Figure 14. The resultant expression,

$$S_G = \frac{TUS}{\sqrt{1 + \frac{c}{W_e}}} \quad , \tag{11}$$

was modified for finite boundaries to the form

$$S_G = \frac{TUS}{\sqrt{1 + \frac{c}{W_e}}} \left(1 - \frac{2c}{W}\right) \quad , \tag{12}$$

where

W = panel width.

This latter expression is analogous to Expression (10) of Crichlow's technique. Although the formulations appear quite different in format, their effectiveness in modeling the data are quite similar due to the nature of the curve-fitting factors implicit to the expressions.

Significance. Although both of these techniques are valid means of representing fracture data, they do not fulfill the dual purpose of a toughness parameter. The effective width, W_e, dimensioned in units of length, defines a "characteristic" but artificial plastic-zone size implicit to the center-cracked panel configuration, but does not relate to a material property other than tensile ultimate strength. The coherent rationale for generalizing this parameter into a broader, more fundamental material characteristic is not evident. While this could be accomplished empirically, it would require an expansive treatise, and, in turn, would defeat the goal of simplicity and generality.

Notch and Crack-Strength Analyses

This approach to fracture characterization has evolved from the concept of notch-stress concentrations at the crack tip (considered a notch with root radius approaching zero). This development is traced in two basic steps discussed in the following subsections.

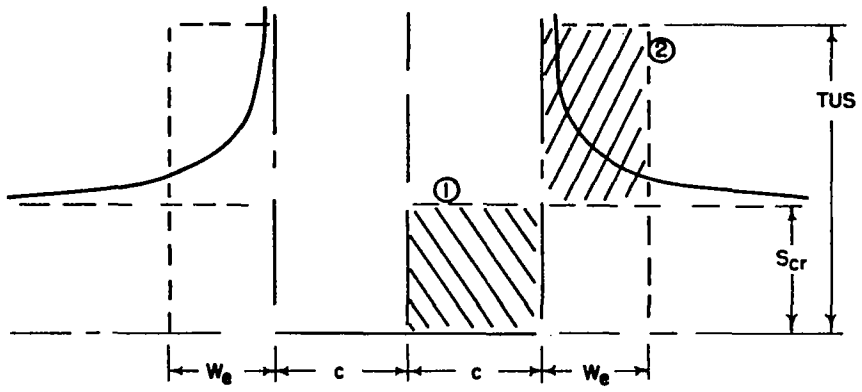

$$S_{cr} \cdot c = W_e \cdot (TUS - S_{cr})$$

Cut Load = Reserve Strength

Area ① = Area ②

FIGURE 13. EFFECTIVE WIDTH FRACTURE MODEL DUE TO CRICHLOW[8]

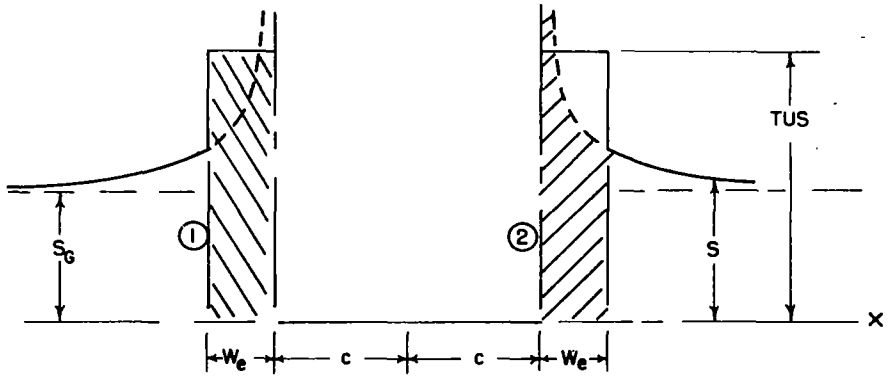

$$TUS \cdot W_e = \int_c^{c+W_e} S\,dx$$

$$S = S_G / \sqrt{1-(c/x)^2}$$

Area ① = Area ②

FIGURE 14. MODIFIED EFFECTIVE-WIDTH FRACTURE MODEL DUE TO CHRISTENSEN AND DENKE[9]

Notch-Strength Analysis (NSA). Current concepts of notch analysis were originally presented by Neuber, who considered the problem in terms of elastic theory and the necessary modification for real materials.[10] Further engineering refinements have been developed by Kuhn and Figge.[11]

Essentially, stress-concentration factors on the net section are modified by size effect (a function of the Neuber constant, ρ') and plasticity. These factors are used with the ultimate strength to define the critical or allowable net section stress based on an initial flaw or crack size. The applicable equations for cracked center-notch specimens are

$$K_u = 1 + 2k_w\sqrt{\frac{c_o E_1}{\rho' E}} \quad , \tag{13}$$

and

$$S_n = \frac{TUS}{K_u} \quad , \tag{14}$$

where

c_o = half crack length before loading

ρ' = Neuber's constant

E = elastic modulus

E_1 = secant modulus at ultimate strength

k_w = Dixon's[12] finite-width correction = $\sqrt{(1 - 2c_o/W)/(1 + 2c_o/W)}$.

TUS = tensile ultimate strength

S_n = critical net section stress = $S/(1 - 2c_o/W)$.

(K_u is the effective net section stress concentration factor).

The similarity of the rightmost term to the basic formulation of the stress intensity factor suggested[13] the consolidation of modulus values and the Neuber constant into one factor termed "crack sensitivity".

Crack-Strength Analysis (CSA). An inverse measure of material toughness termed crack sensitivity was introduced by making the consolidation,

$$C_m = \frac{2}{\sqrt{\rho'}}\sqrt{\frac{E_1}{E}}, \tag{15}$$

in Expression (13) with the resulting net section stress concentration factor,

$$K_u = 1 + C_m k_w \sqrt{c_o} \quad . \tag{16}$$

This expression may be transposed to

$$C_m = \frac{K_u - 1}{k_w \sqrt{c_o}} = \frac{\frac{TUS}{S_n} - 1}{k_w \sqrt{c_o}} \quad , \tag{17}$$

which may be used to evaluate the crack sensitivity directly from experimental data. A typical illustration of the S_n - $2c_o/W$ plot as generated by the crack-sensitivity concept is shown in Figure 15. The solid line represents the average crack-sensitivity line computed for the data in accord with Expression (17). The actual data points are shown as open circle symbols. While the fit is moderately good, the apparent scatter tends to increase with increasing aspect ratio $2c_o/W$. This can be seen very distinctly in Reference 14. It is important to note that, in a qualitative sense, crack sensitivity, C_m, is an inverse K value, i.e., it is inversely proportional to failure stress. High values of C_m denote brittleness; low values of C_m denote toughness.

Significance. The easily grasped physical significance of the stress-concentration-factor concept makes this technique an attractive means of expressing toughness. However, since C_m, as defined by Expression (17), is determined from the net stress, Sn, and the dimensionless aspect ratio, $2c_o/W$, panel width remains a free parameter. This lacks some of the generality sought for in other methods. Again on the positive side, this approach represents "residual" strength in its truest form. Based on initial flaw size and yet relating to failure load, it automatically compensates for the slow crack growth inherent to the rising-load test. This is in contrast to the idealized K concept which is based on a simultaneous correlation of flaw size and stress.

A Generalized Residual-Strength-Analysis Technique

A simplified representation of thin sheet fracture data has been suggested in Reference 15. It combines simplicity of the basic formulation [Expression (2)] of the stress-intensity factor with the direct usefulness of data fits forced by means of the effective-width methods. The development of this method is briefly discussed in the next paragraph.

Development. The major stumbling blocks to the effective utilization of the stress-intensity factor, K, in characterizing fracture data have been the correction factors for plasticity, width, and their combined effect, especially at the extremes of flaw size. On the basis of empirical evidence recited in Reference 15, it has been noted that linear-curve fits are reasonable approximations to the behavior of both the very small flaws at high stress levels and the very long flaws at low stress levels. Furthermore, it was noted that a very consistent and representative fracture index could be achieved by computing a simple stress-intensity factor from the data in the central portion of a stress-flaw size display. As a result, the fracture data are screened in accordance with the criteria:

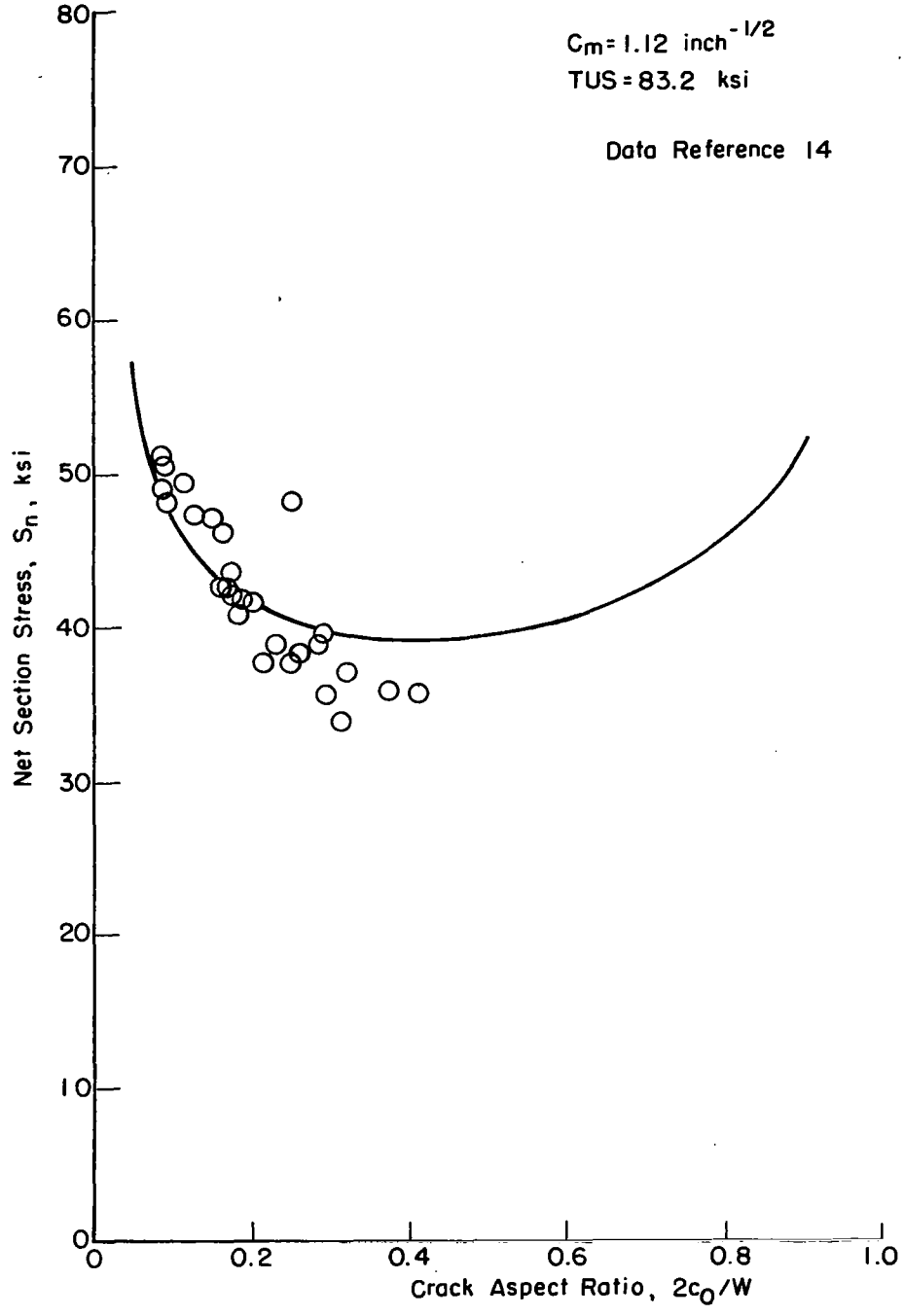

FIGURE 15. FRACTURE DATA FOR 90-MIL-THICK, 12-INCH-WIDE 7075 ALUMINUM ALLOY SHEET DISPLAYED BY THE CSA METHOD

$$S \leq 2\,(TYS)/3 \tag{18}$$

and

$$2c/W \leq 1/3 \quad , \tag{19}$$

to avoid the uncertainties of plasticity and boundary corrections. In essence, this restricts the computational data to the quadrant within the dashed lines of Figure 16. These data are used to calculate a corresponding stress intensity factor as defined by the simple formulation

$$K = S\sqrt{\pi c} \quad . \tag{2}$$

The average value of K is used to determine the central S-2c curve within the quadrant, i.e., from Points A to B. Straight lines to fit the extreme flaw sizes are then drawn from Point A to coordinate (O, TYS) and from Point B to coordinate (W, O). These lines are tangent to the central curve at Points A and B, respectively. In fact, in the original development, the tangency criterion, was the primary basis for selecting the screening Expressions (18) and (19). In essence, the straight-line segments are graphical approximations to plasticity and finite-width corrections.

Justification. As evidence of the applicability of this technique for modeling both threshold- and critical-flaw conditions, Figures 20 through 24 are presented. In these figures, well documented data are displayed along with the line fit by this method.

Figure 17 illustrates fracture data for 0.14-inch-thick 4330 M steel sheet. The data points represent the critical condition $(2c_2, S_1)$ as determined from high-speed photography. This particular curve is determined on the basis of the four data points in the central portion of the figure and are characterized by the value, K = 278 ksi-in.$^{1/2}$. The resultant curve, however, also fits the highest stressed point, thus demonstrating the effectivity of the method.

In Figures 18 and 19, data from two different widths of 0.10-inch-thick 2219-T87 aluminum alloy sheet are presented. The first curve, for 24-inch-panel data, is fit on the basis of the single data point within the defined quadrant, and yet matches related data quite closely. The second curve, for 48-inch-wide-panel data, has a superior fit based on a larger quantity of data. Note that the K values for both widths are quite close together. As in Figure 16, the data points represent the critical instability condition $(2c_2, S_1)$

Cryogenic test data for 2014-T6 aluminum alloy sheet are presented in Figure 20. The curve fit which is extrapolated from the central quadrant into the plastic range as well as toward the boundary edge are considered quite significant.

Finally, consider the larger mass of data shown in Figure 21 for 7075-T6 aluminum alloy sheet. Both threshold, $(2c_o, S_o)$ and critical, $(2c_2, S_1)$, flaw conditions are presented. The fit is quite good and closely matches the results of Reference 14.

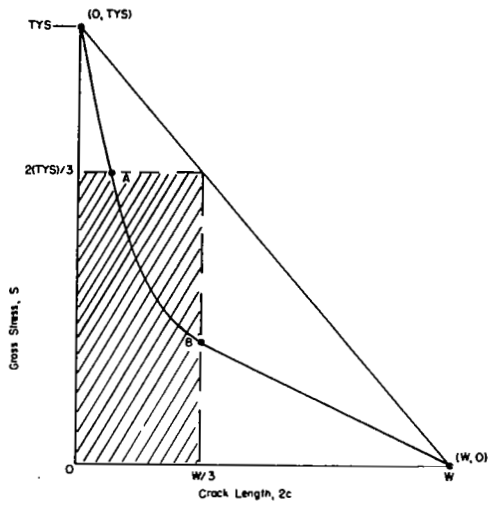

FIGURE 16. FORMAT FOR GENERALIZED RESIDUAL-STRENGTH ANALYSIS

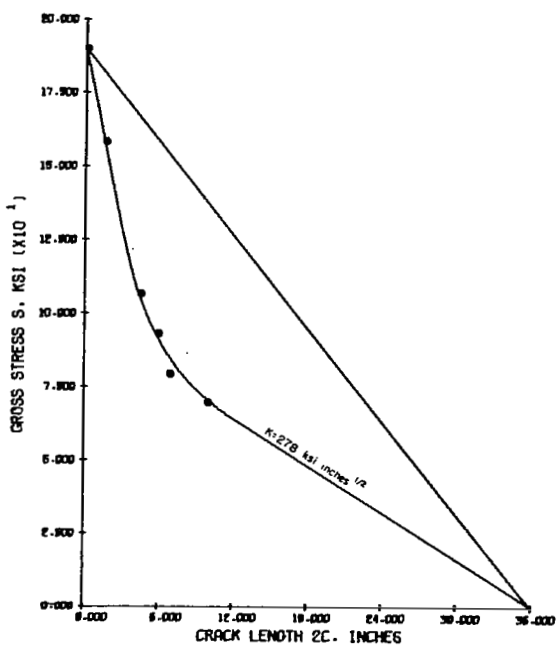

FIGURE 17. FRACTURE DATA FOR 0.140-INCH-THICK, 36-INCH-WIDE 4330M STEEL SHEET[16]

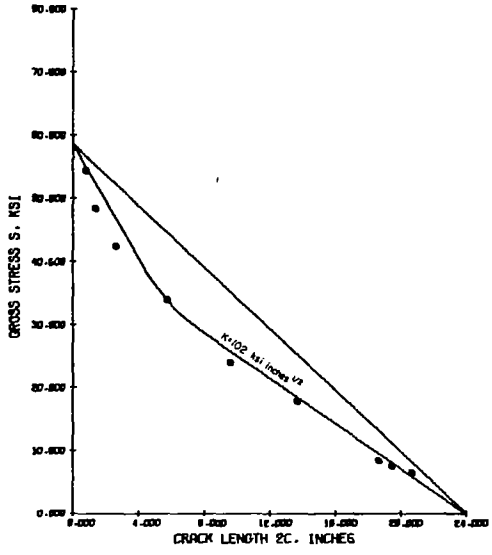

FIGURE 18. FRACTURE DATA FOR 0.10-INCH-THICK, 24-INCH-WIDE 2219-T87 ALUMINUM ALLOY SHEET

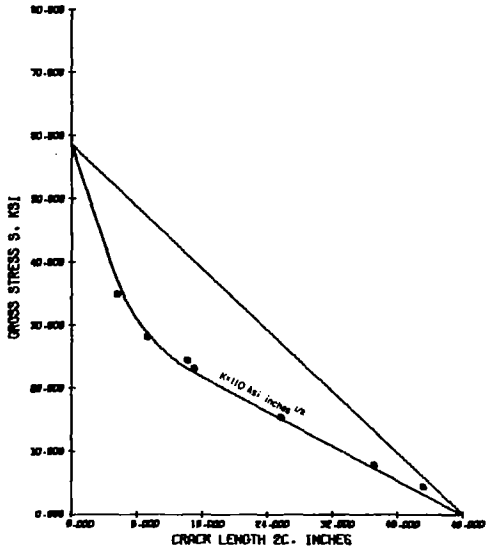

FIGURE 19. FRACTURE DATA FOR 0.10-INCH-THICK, 48-INCH-WIDE 2219-T87 ALUMINUM ALLOY SHEET

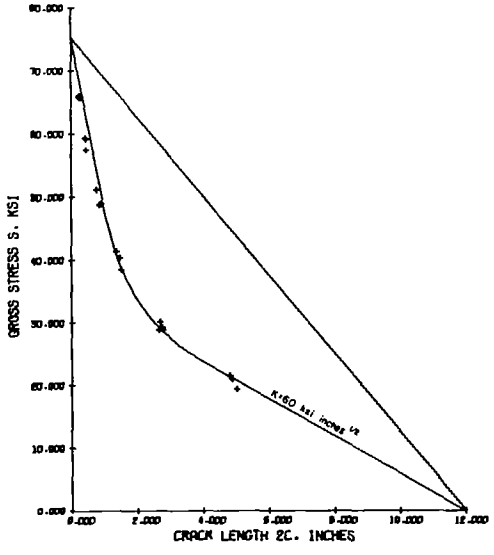

FIGURE 20. FRACTURE DATA FOR 0.060-INCH-THICK, 12-INCH-WIDE 2014-T6 ALUMINUM ALLOY SHEET AT -320 F(17)

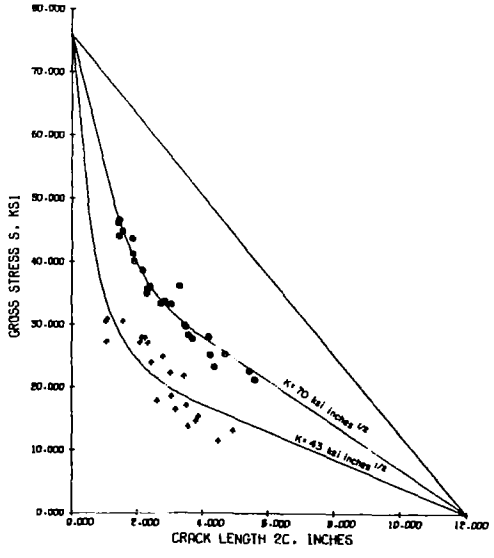

FIGURE 21. FRACTURE DATA FOR 0.090-INCH-THICK, 12-INCH-WIDE 7075-T6 ALUMINUM ALLOY SHEET

Significance. This graphical technique is of value for indexing material toughness and for data displays. For the data of this report (analyzed in the next section) and those of other sources, it appears that this technique models the data quite well for engineering purposes. It combines the essential features of each of the three previously described methods. First, each data group is characterized by a single stress-intensity factor in simple form. Second, a continuous stress-flaw size curve is generated. Third, it exhibits net-section-stress trends with a consistency at least as good as that of crack-strength analysis. This latter point is amply illustrated by Figure 22. The data of Figure 15 (or 21) are presented again in the notch strength format of maximum gross stress and initial flaw size, and analyzed in accordance with the proposed generalized method. The fit is considerably better than that of net-stress format and lends further credence to the soundness and applicability of this method.

Data Analysis

The data derived from this program have been analyzed in terms of stress-intensity factors, crack sensitivity, and residual strength, as previously discussed. These analyses and displays are presented in the following subsections.

Stress-Intensity Factors

A parametric characterization of material toughness is the stress-intensity factor which has evolved from linear elastic-fracture mechanics and was discussed in the Technical Considerations Section of this report. The general foundation of the stress-intensity factor, repeated from Expression (5) is

$$K = S\sqrt{\pi(c + r)}\ f[2(c + r)/W] \quad . \tag{5}$$

For the data generated on this program the plastic zone model of Expression (7),

$$r = \frac{1}{6\pi}\left(\frac{K}{TYS}\right)^2 . \tag{7}$$

and the finite-width correction in the form

$$f[2(c + r)/W] = \sqrt{\sec\frac{\pi(c + r)}{W}} \quad ,^{(1)} \tag{20}$$

were used. The calculation of K for a given data point requires an iterative procedure that was cycled until the convergence of K was within 0.1 percent of the previous value. This required from three to five cycles.

The stress-intensity-factor values for the data generated on this program are presented in Figures 23 through 29. A tabulation of these values is presented in Appendix B. For each specimen, two stress-intensity-factor values were computed by means of the above expressions. First using the initial crack length, $2c_o$, and the five percent secant-offset stress, S_o, a stress intensity factor, K_o, was computed as indicative of the threshold or onset of crack growth. This value is shown as an open triangle

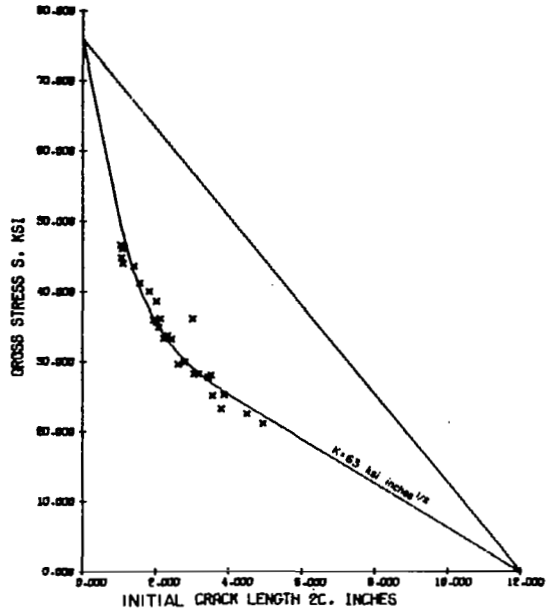

FIGURE 22. FRACTURE DATA ON A NOTCH-STRENGTH FORMAT FOR 0.090-INCH-THICK, 12-INCH-WIDE 7075-T6 ALUMINUM ALLOY SHEET

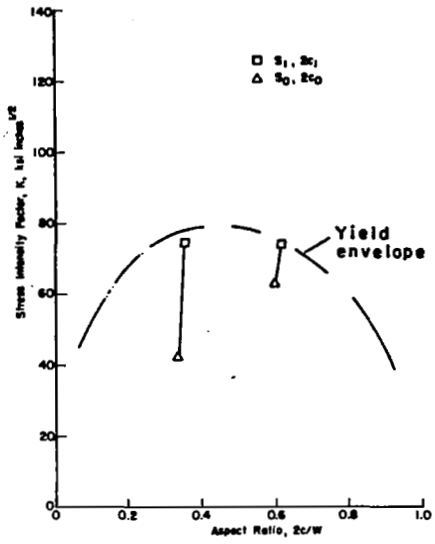

FIGURE 23. STRESS-INTENSITY FACTORS FOR 8-INCH-WIDE, 0.050-INCH-THICK 2024-T3 ALUMINUM ALLOY SHEET

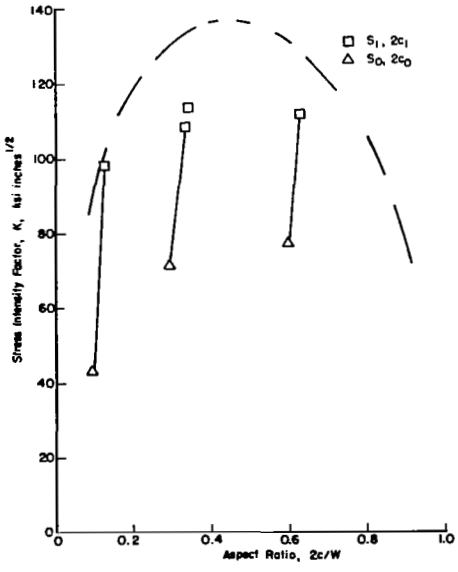

FIGURE 24. STRESS-INTENSITY FACTORS FOR 24-INCH-WIDE, 0.050-INCH-THICK 2024-T3 ALUMINUM ALLOY SHEET

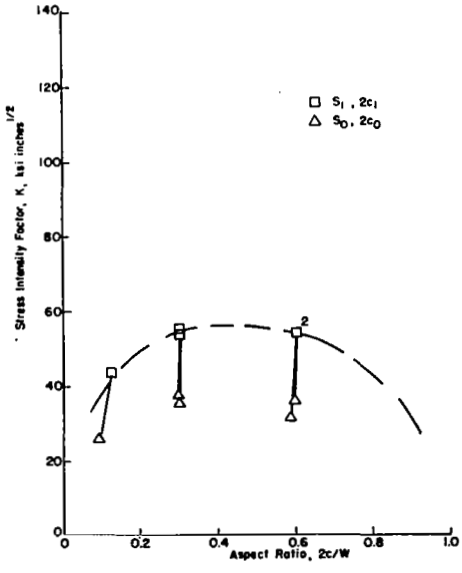

FIGURE 25. STRESS-INTENSITY FACTORS FOR 4-INCH-WIDE, 1/8-INCH-THICK 2024-T3 ALUMINUM ALLOY SHEET

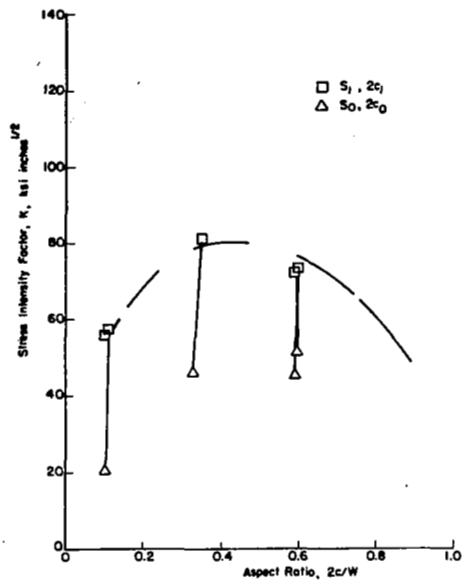

FIGURE 26. STRESS-INTENSITY FACTORS FOR 8-INCH-WIDE, 1/8-INCH-THICK 2024-T3 ALUMINUM ALLOY SHEET

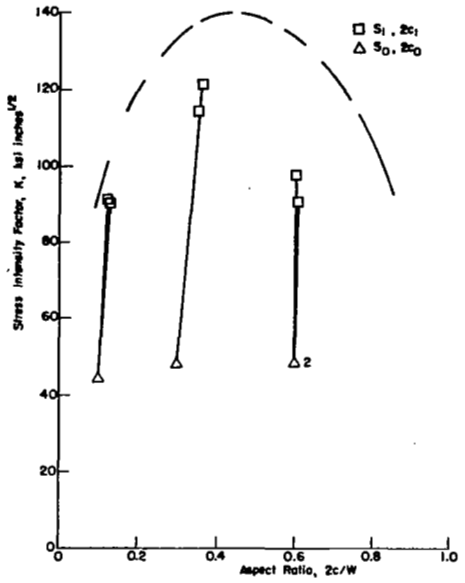

FIGURE 27. STRESS-INTENSITY FACTORS FOR 24-INCH-WIDE, 1/8-INCH-THICK 2024-T3 ALUMINUM ALLOY SHEET

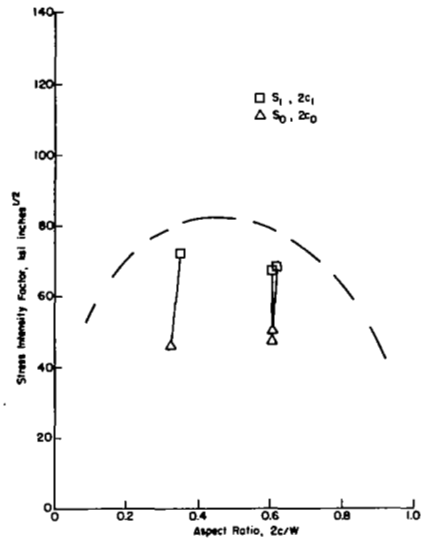

FIGURE 28. STRESS-INTENSITY FACTORS FOR 8-INCH-WIDE, 1/2-INCH-THICK 2024-T3 ALUMINUM ALLOY PLATE

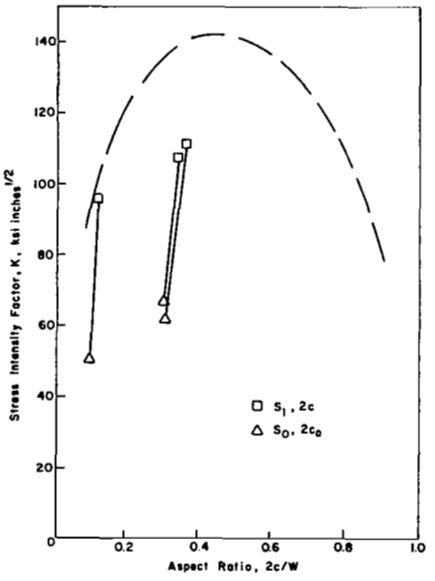

FIGURE 29. STRESS-INTENSITY FACTORS FOR 24-INCH-WIDE, 1/2-INCH-THICK 2024-T3 ALUMINUM ALLOY PLATE

on the figures. A second value, using the crack length, $2c_1$, at the end of slow growth, and the maximum load stress, S_1, was calculated and denoted K_1. The value is associated with the critical-fracture condition and is shown in the figures as an open-square symbol. Corresponding values for a single specimen are shown as connected pairs.

A third value using the crack length $2c_2$ was attempted, but, in most instances, diverged, illustrating the limitations of the elastic model. This is further emphasized by the proximity of the yield envelope shown as a dashed curve on all of the figures.

Crack Sensitivity

The data of this program were also analyzed in accordance with the crack-strength-analysis (CSA) method described earlier in this report. The initial crack length, $2c_o$, and maximum fracture stress, S_1, were utilized in determining individual crack-sensitivity values, C_m, for each specimen. These values were calculated by means of Expression (17) and are tabulated in Appendix B, where both individual and average values are presented for each combination of width and thickness. The average values from Appendix B are displayed in graphical form on Figure 30. It should be noted that the results of this data analysis technique appear to be quite consistent for the 8 and 24-inch-wide panels for all three thicknesses. An overall average value of $C_m = 0.616\text{-in.}^{-1/2}$ was computed for these cases. The deviation of the 4-inch-wide panels is believed to be due to boundary effects and the stronger influence of gross plasticity.

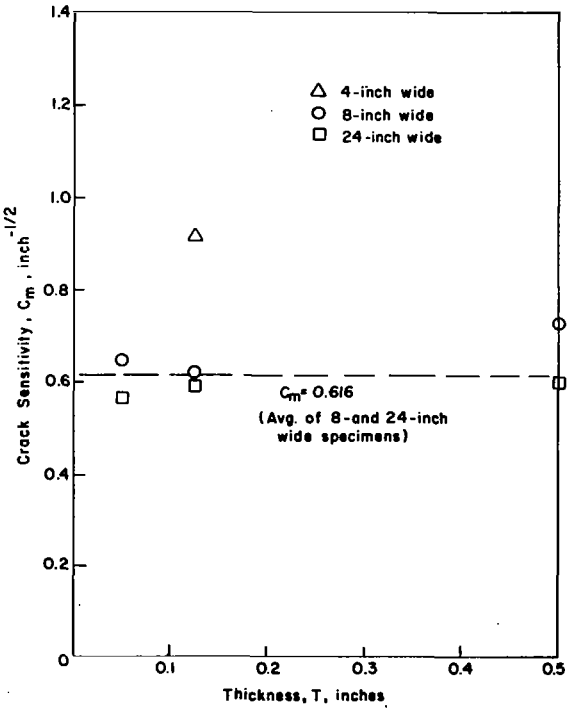

FIGURE 30. AVERAGE CRACK SENSITIVITY VALUES FOR 2024-T3 AND -T351 ALUMINUM ALLOY SHEET AND PLATE

As illustrative of the effectiveness of the CSA method in modeling fracture data, Figure 31 has been prepared. By using the above-noted average C_m value and an average tensile ultimate strength,

$$TUS = 71.5 \text{ ksi} \quad ,$$

the relation of net section stress S_n, to initial crack aspect ratio, $2c_o/W$, has been computed by the expression

$$S_n = \frac{TUS}{C_m K_w \sqrt{c_o} + 1} \quad ,$$

a transformation of Expression (17), and has been plotted as a solid line for both 8- and 24-inch-wide panels.

Residual Strength

The generalized residual-strength analysis technique which was discussed previously in this report has been used to analyze the data generated on this program. The results are presented graphically in Figures 32 through 38. In these figures, the triangular symbols (Δ) denote the data coordinates, $(2c_o, S_o)$, characteristic of the threshold of slow growth. The "plus" symbols (+) denote the data coordinates, $(2c_1, S_1)$, characteristic of the end of slow growth, or the lower limit to rapid fracture. The circular symbols (O) denote the data coordinates, $(2c_2, S_1)$, the upper limit to the critical fracture condition. Since the fracture data of this program are not as extensive as those of the program on which the technique was developed, the curve fits are not as broadly based. However, it is believed that when these data are analyzed along with a larger data reservoir, the significance of this picture will be more apparent. In general, the threshold data points exhibit considerable scatter because of inherent experimental inaccuracies. Recognizing that mechanical-offset determinations are a conservative means of identifying growth, especially at small crack lengths, an average K value of 40 ksi-in.$^{1/2}$ appears to be representative. While the critical fracture condition is closely associated with net section yielding, the wide panels (24-inch) appear to exhibit a characteristic stress-intensity factor, K, of about 100 ksi-in.$^{1/2}$.

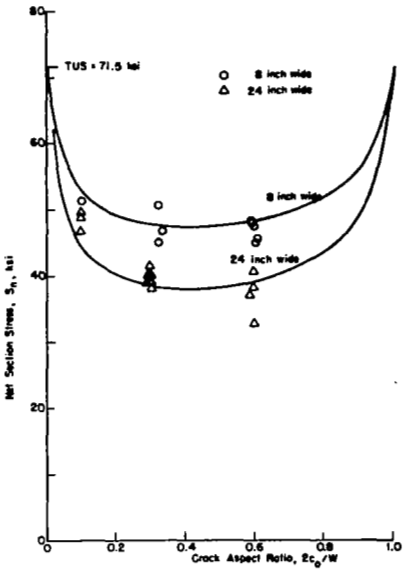

FIGURE 31. FRACTURE DATA FOR 2024-T3 AND -T351 ALUMINUM ALLOY SHEET AND PLATE PRESENTED ON CSA FORMAT

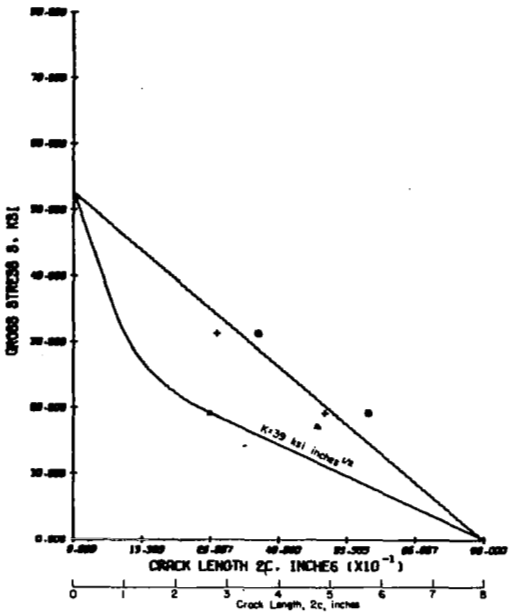

FIGURE 32. FRACTURE DATA FOR 0.050-INCH-THICK, 8-INCH-WIDE 2024-T3 ALUMINUM ALLOY SHEET

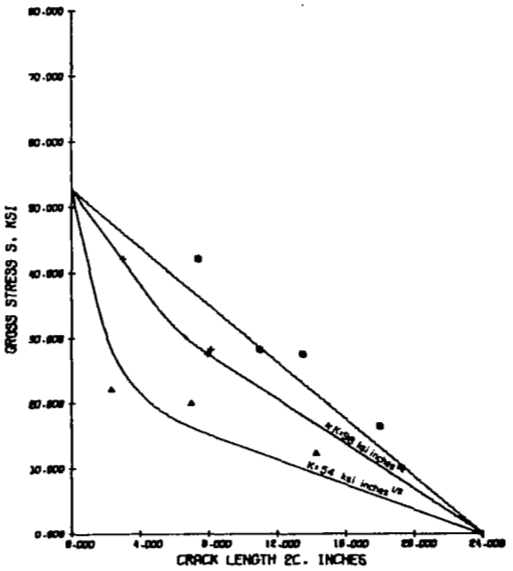

FIGURE 33. FRACTURE DATA FOR 0.050-INCH-THICK, 24-INCH-WIDE 2024-T3 ALUMINUM ALLOY SHEET

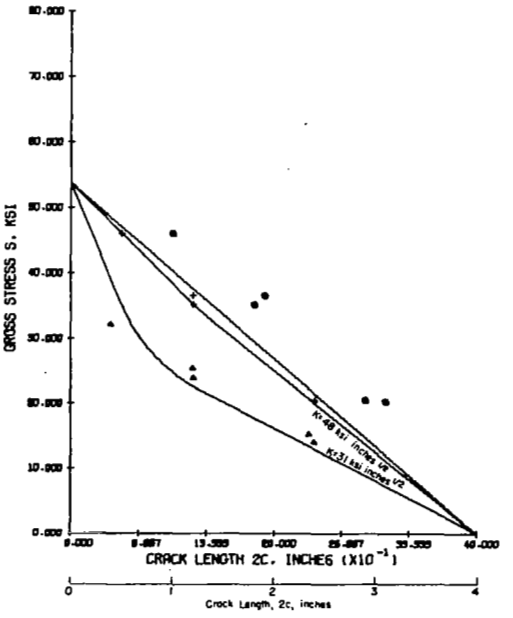

FIGURE 34. FRACTURE DATA FOR 1/8-INCH-THICK, 4-INCH-WIDE 2024-T3 ALUMINUM ALLOY SHEET

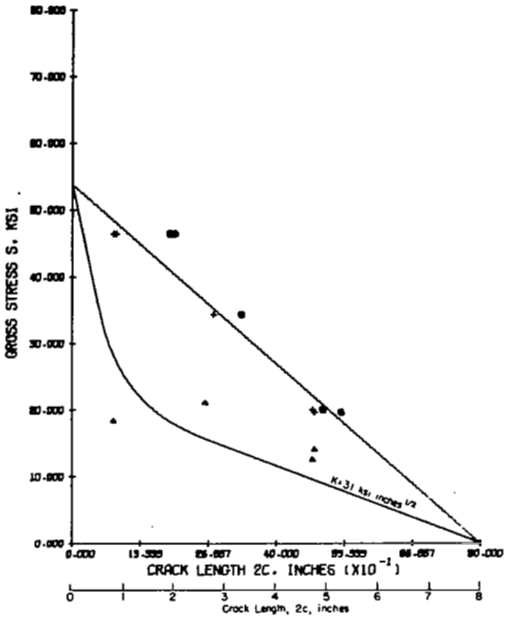

FIGURE 35. FRACTURE DATA FOR 1/8-INCH-THICK, 8-INCH-WIDE 2024-T3 ALUMINUM ALLOY SHEET

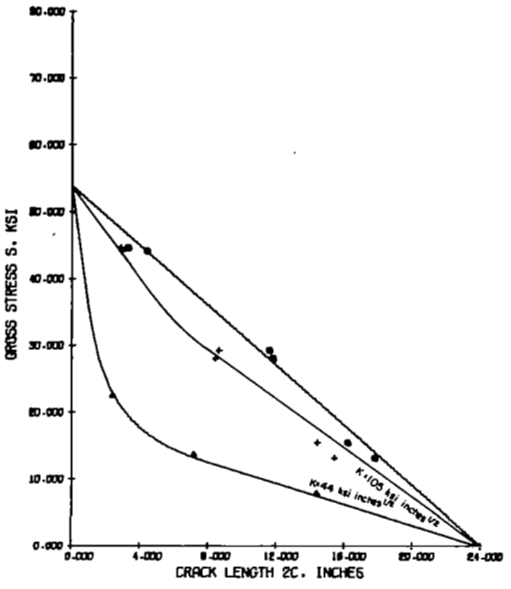

FIGURE 36. FRACTURE DATA FOR 1/8-INCH-THICK, 24-INCH-WIDE 2024-T3 ALUMINUM ALLOY SHEET

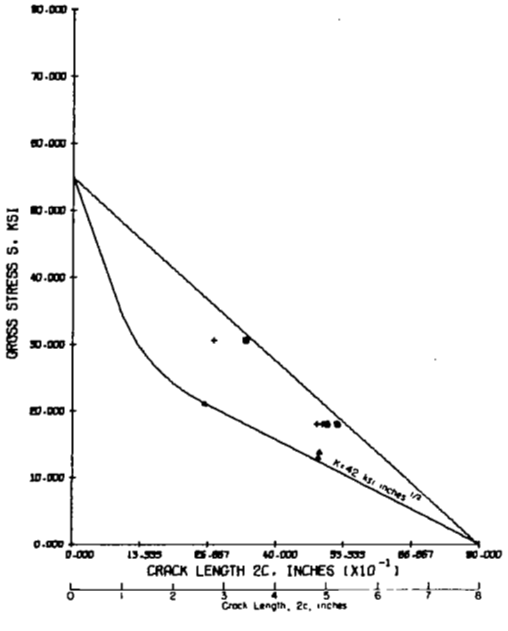

FIGURE 37. FRACTURE DATA FOR 1/2-INCH-THICK, 8-INCH-WIDE 2024-T351 ALUMINUM ALLOY PLATE

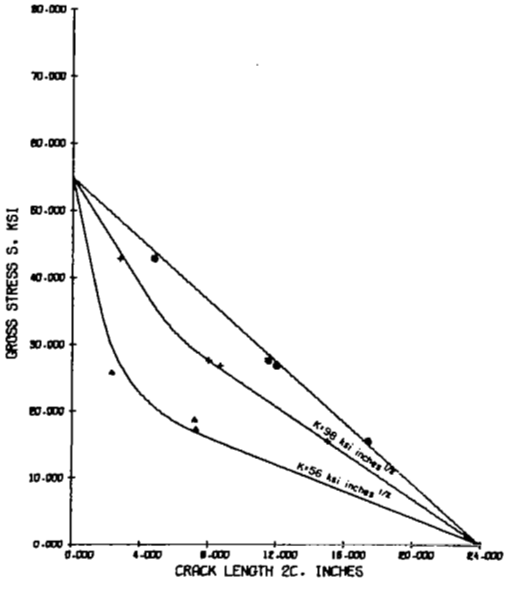

FIGURE 38. FRACTURE DATA FOR 1/2-INCH-THICK, 24-INCH-WIDE 2024-T351 ALUMINUM ALLOY PLATE

THEORETICAL ANALYSES AND IMPLICATIONS

It has long been recognized that crack propagation in structural materials involves plastic strains. However, in relatively "brittle" materials this plasticity is confined to very small regions at the ends of cracks, and it is possible to apply a Griffith type of theory for crack propagation which involves only consideration of elastic stress fields. With more "ductile" materials such as the 2024-T3 aluminum alloy of this program, plastic-zone sizes become comparable with the crack length. Thus a more detailed analysis is required to adequately describe the fracture process.

Two analytical approaches to the problem were tested against the experimental plastic-zone and fracture data. These were a Dugdale model, as developed for finite-width plates, and finite-element analysis for elastic-plastic plane-stress calculations. Both involved application of existing computer programs at Battelle, and represented two well known analysis techniques. The following sections include a brief background on the methods, followed by numerical results with correlation with experimental data. While the plastic-strain field in a cracked plate is truly three dimensional, since the deformation pattern has variations not only in the plane of the plate but also through the thickness, analyses which account for only one or two dimensional plastic zones have often proven valuable in studies of the fracture process. In this program it was determined that the Dugdale-model was inadequate in predicting either the plastic zones or the load to produce yielding across the entire plate cross section. The two-dimensional finite-element analysis predicted these two aspects quite well, but was judged inadequate in predicting strain fields very near the crack tip and thus did not serve well as a basis for a crack-extension criterion.

Analysis of Specimens Using Dugdale Model

The Dugdale model has often proven to give a useful account of the plastic deformation that occurs at the end of a crack under conditions of plane stress. The essential features of the model are shown in Figure 39 for a finite-width plate. In particular the plastic zone is taken as a thin extension of the crack itself, and the length of this zone is adjusted to eliminate the stress singularity at the tip of the extended crack. The advantage of this approach is that the linear theory of elasticity can be applied since, in the analysis, the plasticity near the crack tip is represented simply as a loading equal to the material yield stress which is applied to the edges of the extended slit.

It was anticipated at the onset of the present study that the Dugdale model could give reasonable predictions of plastic zones and strains for correlation with test data. An existing computer program for analyzing a Dugdale crack in a finite-width plate was used to generate a set of numerical data corresponding to the test conditions. The Battelle-developed program[18] is based on the boundary-point-least-squares method. It had been shown to predict the existence of a maximum load which a finite-width plate can carry before the plastic zone grows to the edge of the plate. These predictions had also been shown to agree with experiment for 0.00175-inch-thick mild-steel foil.

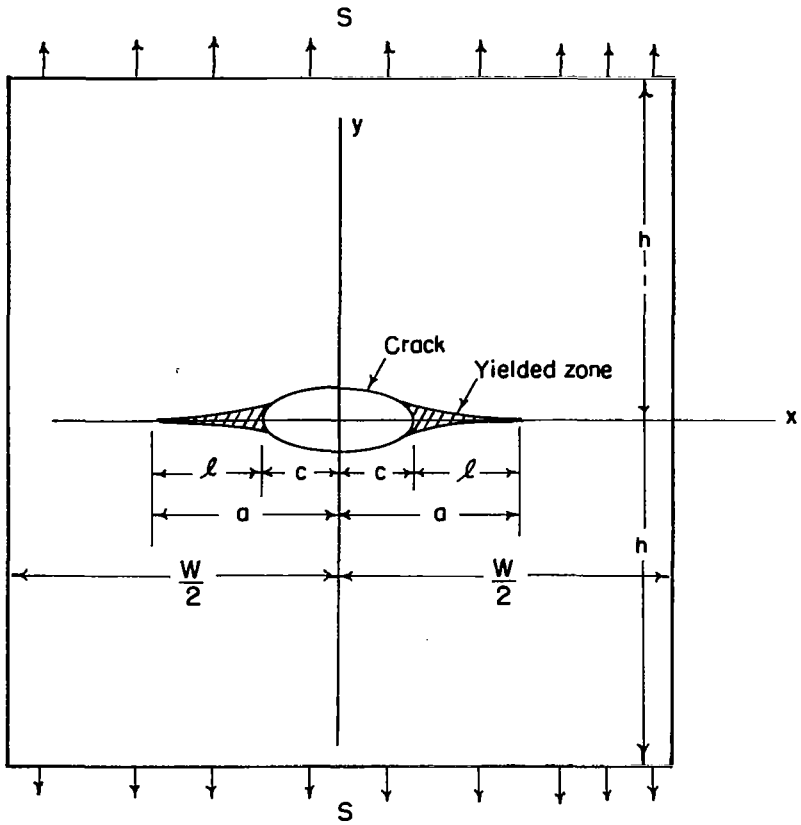

$$S = \frac{2}{W}\int_0^{\frac{W}{2}} [\sigma_y]_{y=h}\, dx$$

FIGURE 39. THE DUGDALE MODEL FOR A CENTRALLY LOCATED CRACK IN A RECTANGULAR PLATE

Numerical Computations

With the available computer program for the analysis of a Dugdale crack in a finite-width plate, a sufficient number of cases was solved to cover the range of loads and crack lengths encountered in the experimental studies. In particular, the following crack aspect ratios were selected

$$2c/W = 1/10,\ 1/5,\ 1/3,\ 1/2 \quad ,$$

and plastic zone sizes were calculated for a minimum of six different applied stress levels for each. In all of the calculations a non-strain-hardening material was assumed. For purposes of computation a plate width of W = 8.0 in. was selected, although it should be understood that the same results would hold for any geometrically similar

plate. The plate length was set at 2h = 12.0 inches, and the boundary conditions at $y = \pm h$ were $\sigma_y = S$ and $\tau_{xy} = 0$. A preliminary check showed that use of a uniform-displacement boundary condition (fixed grips) gave only slightly different results. Also the uniform-traction condition proved a somewhat easier condition to treat from the standpoint of numerical accuracy.

The procedure used in the computer calculations was as follows. A given crack aspect ratio was selected and a unit tensile stress applied. Then a series of progressively longer plastic zones (ℓ in Figure 39) were assumed. For each zone size a corresponding yield stress Y was calculated, and this way the variation of zone size with the applied stress ratio S/Y was determined. At the same time stress and displacement distributions were obtained. Here S is the applied or gross stress and is calculated as load divided by the product of width and thickness.

Figures 40 through 42 are parametric curves plotted on the basis of the limited number of cases analyzed. These give as a function of net stress, the plastic-zone size and the crack-opening displacements at the tip and center of the crack. Net stress was used as a coordinate here to allow plotting of curves for different aspect ratios with a common scale.

The essential character of the zone-size variation with load as predicted by the Dugdale analysis is clear from Figure 40. The requirement that the stress be finite at the end of the plastic zone gives a decreasing load with zone size when the zone approaches the edge of the plate. A certain maximum load for each 2c/W exists, and this implies that the plastic zone propagates to the edge for a small increase in load. The maximum load, termed the tensile instability load, is the maximum load that the plate can carry as predicted by the theory.

Figures 41 and 42 summarize the calculations of crack-tip displacements and displacement at the center of the crack. Here again the curves reach an apparent maximum at the tensile-instability load.

Figure 43 represents a summary of the previous curves. The tensile-instability line is obtained by plotting the maximums of Figure 40. The Dugdale analysis thus suggests that combinations of crack length and load which plot below the curve represent stable zones, and points above the curve, the fully plastic states. Crack-tip displacement, v_c, is a measure of the maximum strain, and is also a possible criteria for extension. Lines of constant values of Ev_c/Y are shown on Figure 43, and these show the same downward trend with increasing crack size as shown by the tensile instability curve.

Comparison of Preliminary Experimental Results With Dugdale Analysis

As reported in Reference 18, plastic-zone predictions of Battelle's boundary-point-least-squares computer program agreed well with experiment for mild-steel sheet. It had been anticipated that similar agreement would be obtained for the 2024-T3 aluminum alloy.

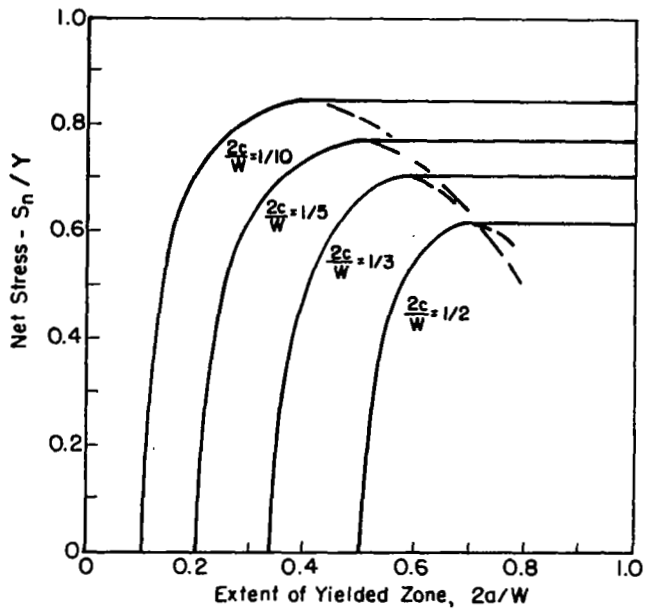

FIGURE 40. PLASTIC-ZONE-SIZE PREDICTION OF DUGDALE ANALYSIS FOR FINITE-WIDTH PLATE

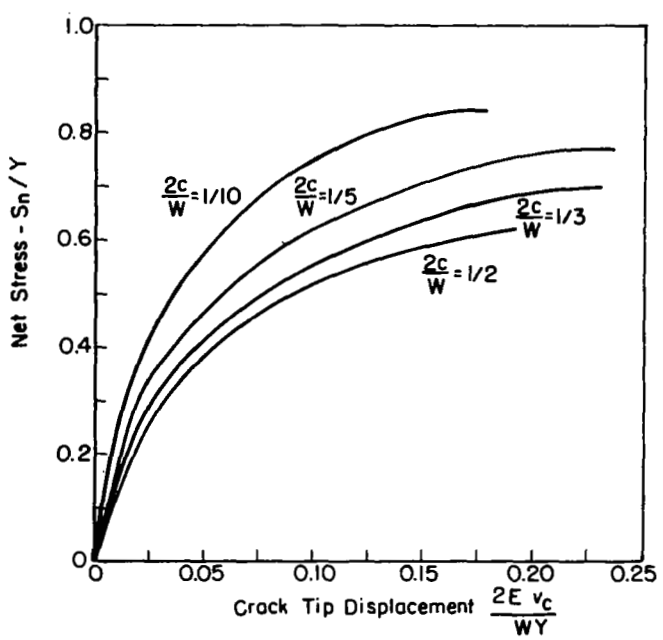

FIGURE 41. CRACK-TIP DISPLACEMENT PREDICTED BY DUGDALE ANALYSIS FOR FINITE-WIDTH PLATE

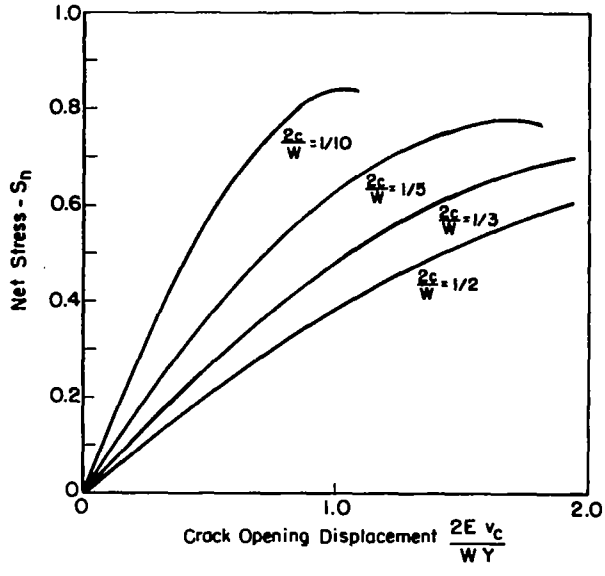

FIGURE 42. CRACK-OPENING DISPLACEMENT PREDICTED BY DUGDALE ANALYSIS FOR FINITE-WIDTH PLATE

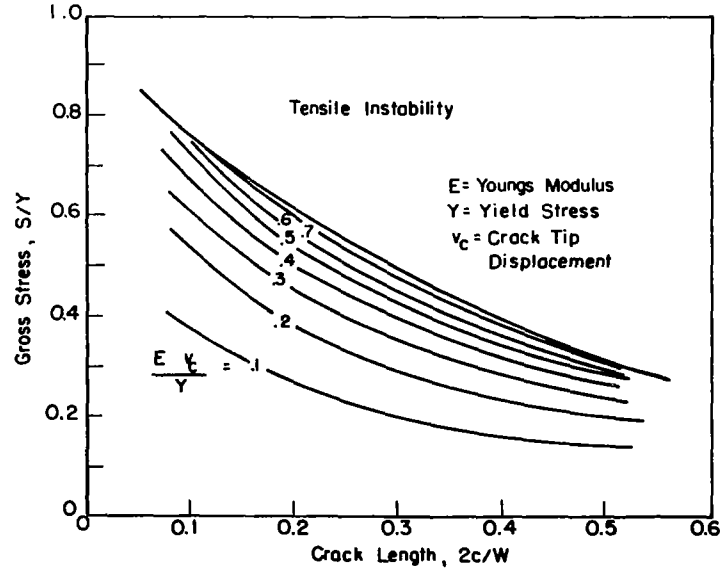

FIGURE 43. CRACK-TIP DISPLACEMENT AND TENSILE INSTABILITY OF DUGDALE PLASTIC ZONE

(Plate Width, W = 8.0", Plate Length, 2h = 12.0")

Preliminary crack-growth data points were plotted for comparison with the tensile instability curve of Figure 43, and the result is shown in Figure 44. Each data point represents an observed combination of crack length (plotted as aspect ratio) and gross stress. Crack lengths recorded are both the extended length just prior to final fracture and the length just before slow growth could be observed visually.

As is clear in Figure 44, all data points fell above the tensile-instability or maximum-load prediction of the Dugdale analysis. If such an analysis were valid all points should lie either on or below the curve. If the maximum load is governed by growth of the plastic zone to the edge of the plate, then the data points should lie on the curve. If fracture occurs due to some critical strain developing at the crack tip, then the data points should fall below the curve. The predicted plastic zones of the Dugdale analysis were too long. Also observations of the surface appearance of the specimens suggested that the zone had the characteristic "hinge" or "butterfly" shape rather than the assumed slit-like form.

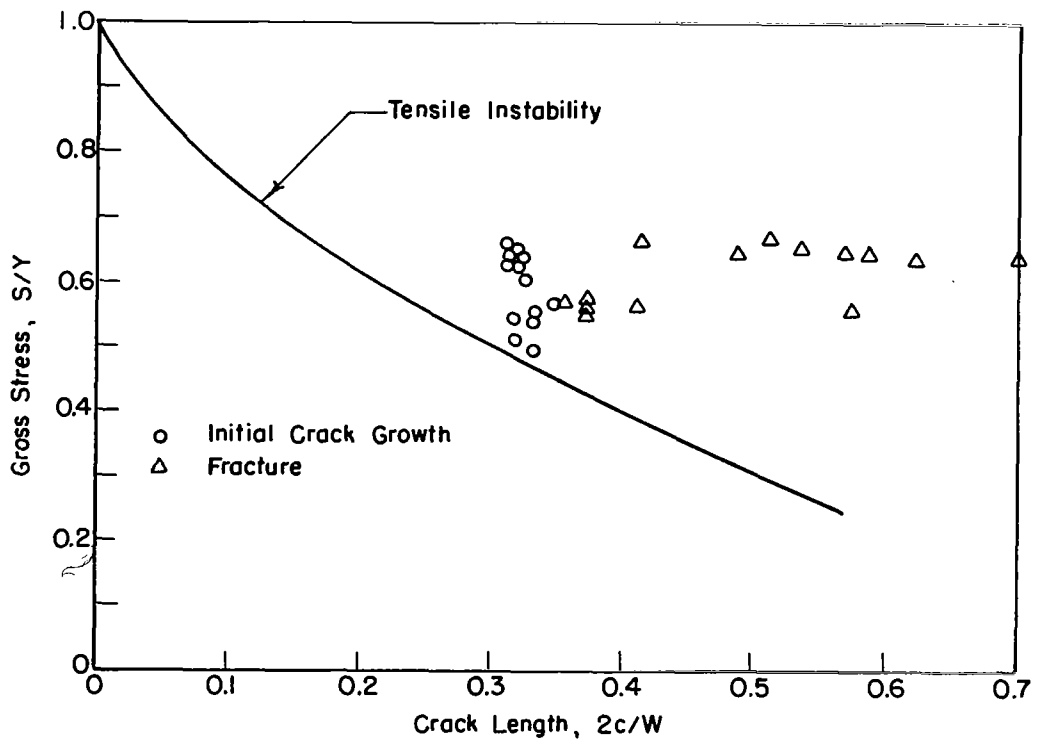

FIGURE 44. PRELIMINARY CRACK-GROWTH DATA RELATED TO TENSILE-INSTABILITY LOAD OF DUGDALE MODEL

It was originally proposed to extend the finite-width-plate computer program to include effects of strain hardening. A strain hardening model would predict a shorter plastic zone and higher maximum load. With the ultimate strength of 2043-T3 about 20 percent higher than the yield strength, it was believed that this alone would not be sufficient correction. Moreover, the zone shape of the Dugdale model was known to be incorrect. Thus, it was concluded that no refinement was justified. Since the Dugdale model proved inadequate, work was directed instead to two-dimensional models.

The reason for the appearance of the Dugdale type of zone in some materials and not others is subject to debate. However, materials with an upper and lower yield stress or with a lack of strain hardening seem more likely to show slit-like zones. The stress strain curve of the 2024-T3 has neither of these characteristics.

Two-Dimensional Analysis of Plastic Zones by Finite-Element Method

In the Dugdale model the plastic zone at the end of a crack is assumed to be a narrow slit-like region. Since initial observations suggested that the plastic zones in the 2024-T3 alloy were not of this shape, a different theory was needed. Such a theory should involve a two-dimensional plastic-zone shape, and preferably should predict this shape as part of the analysis. Battelle's finite-element computer program FEELAP for elastic-plastic analysis of plane-stress states is capable of such predictions, and this existing analysis technique was therefore applied to the plastic-zone problem. Battelle's FEELAP computer program is typical of the constant-strain-element analysis which has found widespread use. Finite-element analyses have been applied to the elastic-plastic crack problem before, notably by Swedlow[19], and the limitations of the method for crack problems should be interpreted with caution. However, in this study, the main interest was in plastic-zone growth, and the load needed to propagate the zone to the edge of the specimen. For this, the finite-element method is quite adequate. The next section describes the computations made using the computer program FEELAP, which is Battelle's version of the program originally developed by Marcal and King.[20]

Numerical Computations

Plastic zones were computed with the finite-element program FEELAP for crack aspect ratios of $2c/W = 1/3$, $1/2$ and $2/3$. The plate width and length were taken as 8.0 and 12.0 inches, and the loading was prescribed as a displacement or fixed-grip condition. In each calculation the applied load was increased until the plastic zone propagated to the edge of the plate.

A bilinear stress-strain curve with strain hardening was prescribed and this was based on tensile data for the 0.123-inch-thick material whose yield strength was about 52,150 psi. Young's modulus and Poisson's ratio were taken as 10.6×10^6 psi and 0.333, respectively.

The finite-element representation of the cracked specimen is shown in Figure 45, with a total of 208 nodal points and 364 elements. Only one quadrant of the symmetric problem was analyzed. About 1 minute of central processor time was required per plastic load increment on Battelle's CDC 6400 digital computer. About 15 load increments were required to analyze each case.

The calculated load-deflection curves are shown in Figure 46 for each of the three aspect ratios. Load is here represented as net section stress normalized with respect to material yield strength. The change in slope occurs when the net section stress is somewhat greater than yield and this is an indication of the gross yielding of the cracked plate. Net section stresses greater than yield were also observed experimentally.

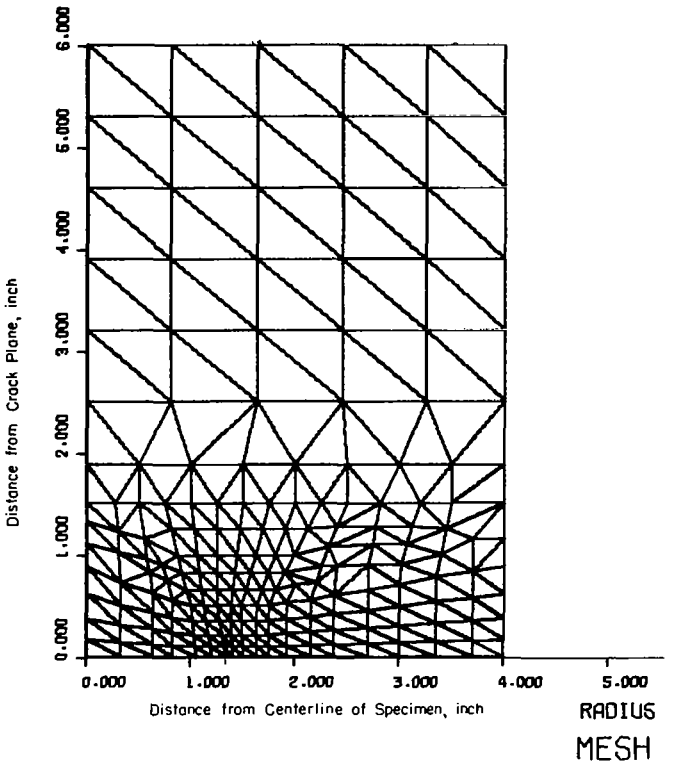

FIGURE 45. FINITE-ELEMENT GRID WORK FOR ASPECT RATIO 2c/W = 1/3

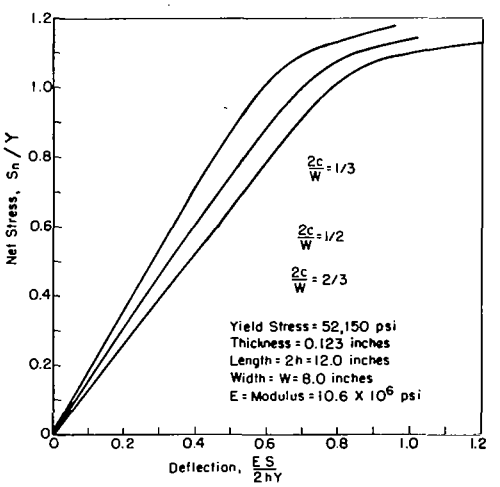

FIGURE 46. CALCULATED LOAD-DEFLECTION CURVES FOR VARIOUS CRACK-ASPECT RATIOS

The predicted shapes and progressive growth of the plastic zones at the end of the crack are shown in Figures 47, 48, and 49, for each of the three crack aspect ratios. Some judgment was required in locating the contours precisely, since each finite element of the grid was either elastic or entirely plastic because of the assumption of constant strain within an element. The movement of the elastic-plastic boundary was thus discontinuous. The zone shapes are labeled according to the net cross-sectional stress.

Some aspects of the plastic-zone growth can be noted. Referring to Figure 47 for $2c/W = 1/3$ it is seen that the zone has extended hardly more than half way to the edge of the plate, even though the net stress of 52,500 psi is greater than yield. However, at a slightly higher stress of 56,400 psi, the zone has moved to the edge of the plate. For all aspect ratios the zone grew very slowly at low stress levels, and then showed a very rapid increase in growth rate as the net section yield stress was approached.

The zone shapes predicted were very much two dimensional, and had a "butterfly" appearance. In this respect they were quite different from the slit-like zone of the Dugdale model. Viewing Figures 47 to 49 successively, it is seen that the zone assumes a more rounded appearance for larger crack aspect ratios.

Photoelastic Determination of Plastic Zones

A number of methods are available to determine the region of plastically deformed material at the ends of cracks. Etching techniques give a positive indication of plastic deformation but they are applicable to only a few materials. For two-dimensional specimens, plane-stress conditions are usually assumed, and yield is evident as changes on the specimen surface. Yield zones are often estimated on the basis of surface appearance as was done during the early tests. Replication techniques can give quantitative measurements of thickness changes, and perhaps a more precise indication of yield.

The photoelastic coating method used in the present work is believed to be more precise than some of the alternative methods. The coating technique and the series of measurements made are described after discussing the theoretical basis for the photoelastic plastic-zone determinations.

The photoelastic coating method used in this program is believed to be more precise than some of the alternative methods. The theoretical basis for the photoelastic plastic-zone determination, the techniques employed, and the results are given in Appendix C. The correlation of the photoelastic measurements with calculations described in the previous section was examined as described in the next section.

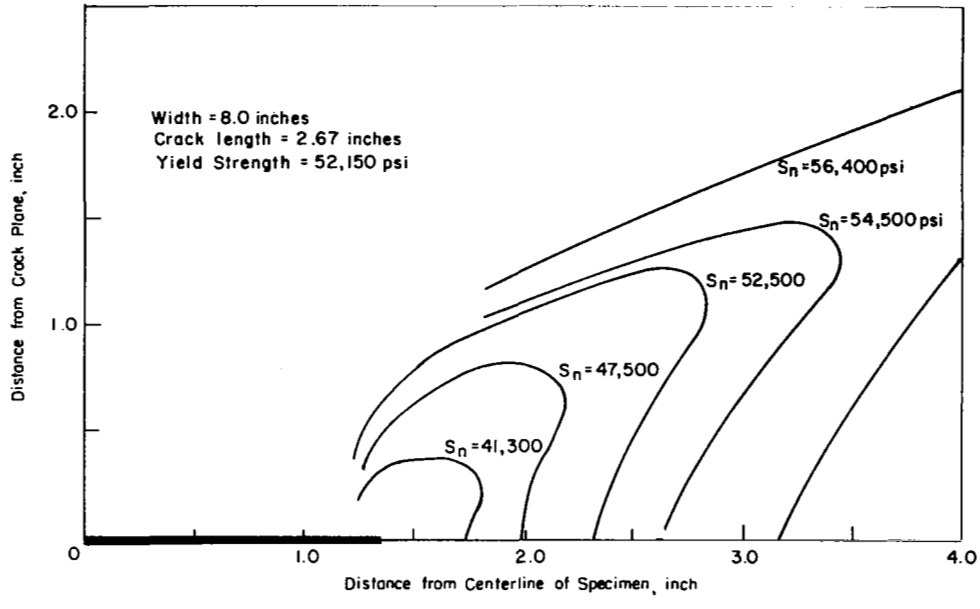

FIGURE 47. PLASTIC ZONE IN 2024-T3, 0.125-INCH-THICK SPECIMEN AS DETERMINED BY FINITE-ELEMENT CALCULATION, 2c/W = 1/3

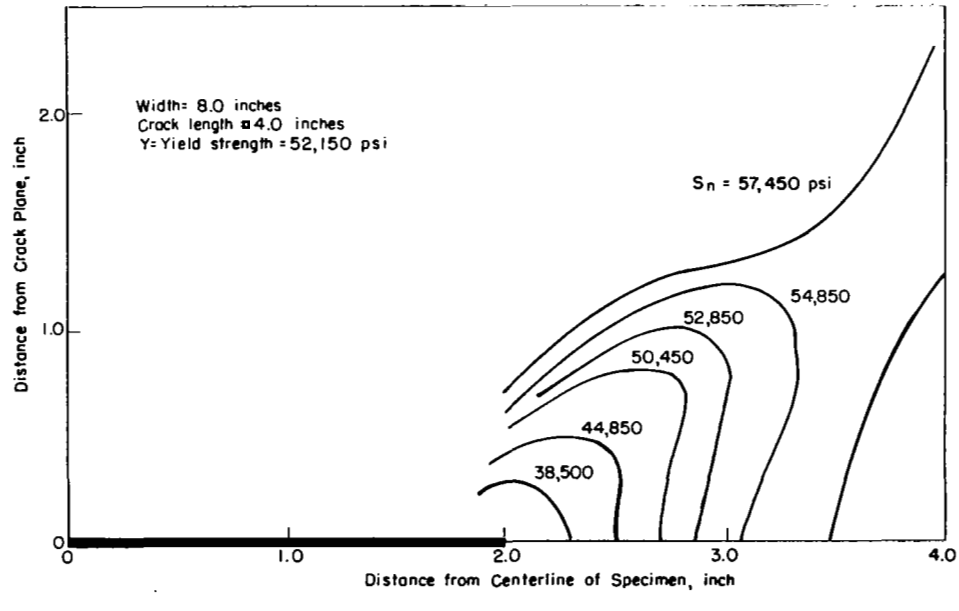

FIGURE 48. PLASTIC ZONE IN 2024-T3, 0.125-INCH-THICK SPECIMEN AS DETERMINED BY FINITE-ELEMENT CALCULATION, 2c/W = 1/2

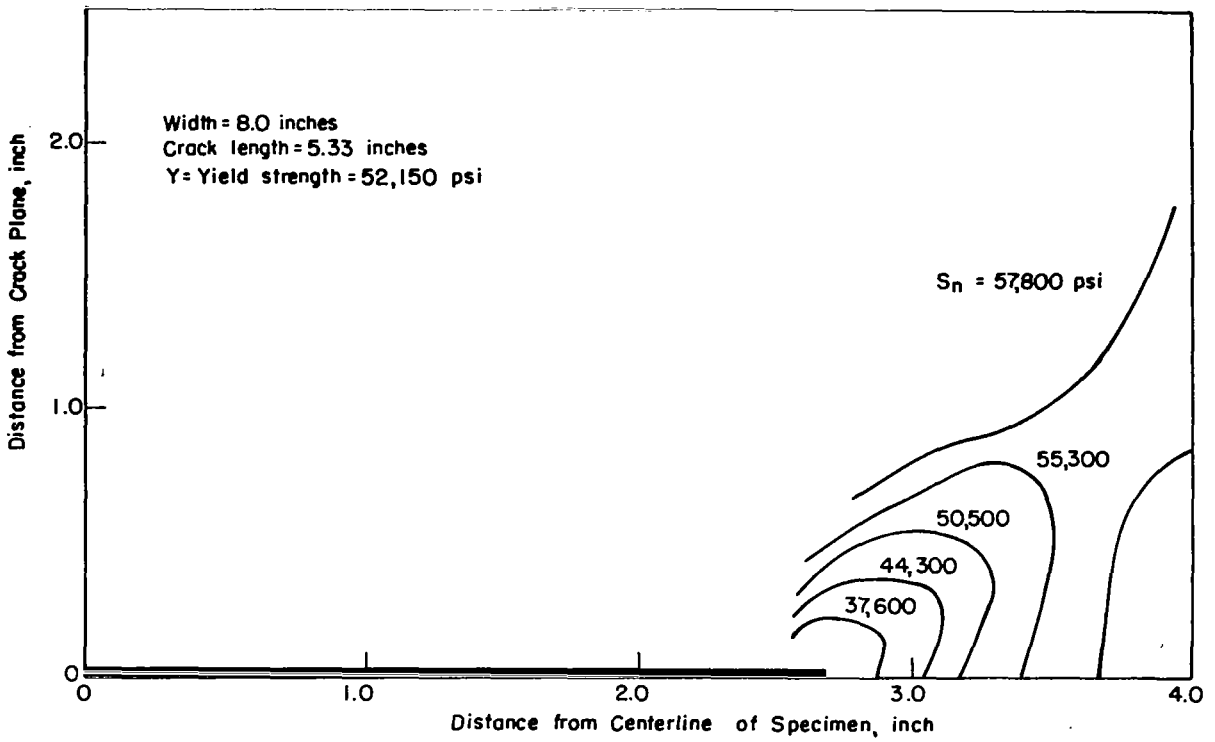

FIGURE 49. PLASTIC ZONE IN 2024-T3, 0.125-INCH-THICK SPECIMEN AS DETERMINED BY FINITE-ELEMENT CALCULATION, 2c/W = 2/3

Correlation of Calculated and Measured Plastic Zones

The agreement between the calculated and experimentally determined plastic zones was examined. However, as a preliminary check, the calculated and experimental strain fields were compared as shown in Figure 50. The strain-difference lines (as photoelastically determined) are shown as solid contours and the calculated strain differences by dash contours. In general the agreement is quite good.

The photoelastically determined plastic zones for the four coated specimens are shown in Figures 51 through 54. They show the same characteristic "butterfly" shape as those predicted by the finite-element plane-stress calculations. For all except the 24-inch-wide specimen, zone growth to the edge of the plate was recorded prior to fracture. For the 24-inch specimen of Figure 54, the last photoelastic record was at a stage when the zone was growing very rapidly, so the zone may have subsequently spread to the edge of the plate at a slightly higher loading. Initial stages of slow crack growth is evident in Figure 53, as a shifting of the zones to the right.

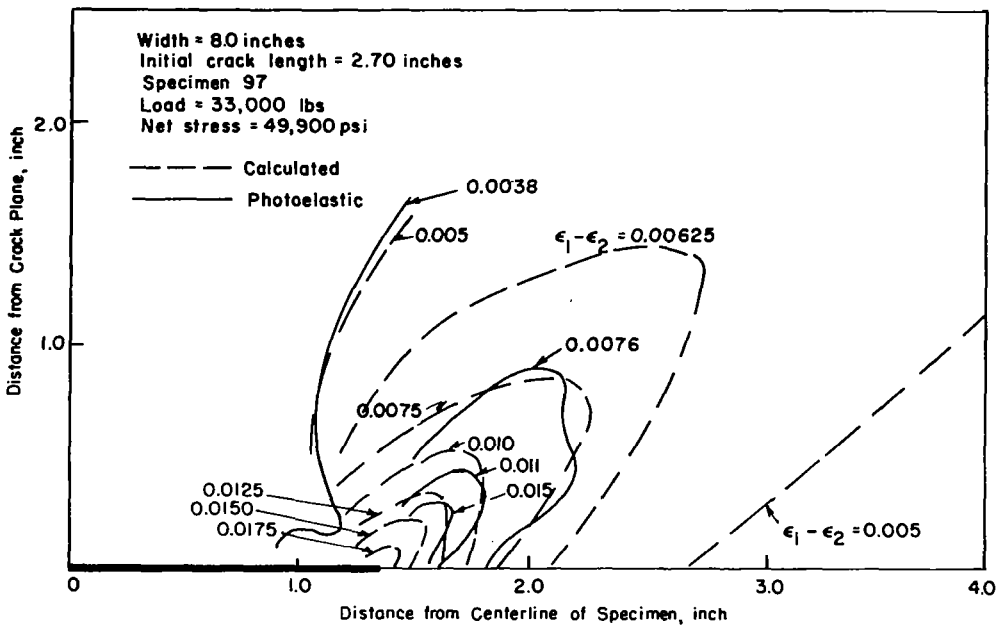

FIGURE 50. COMPARISON OF MEASURED AND CALCULATED DISTRIBUTIONS OF PRINCIPAL STRAIN DIFFERENCE

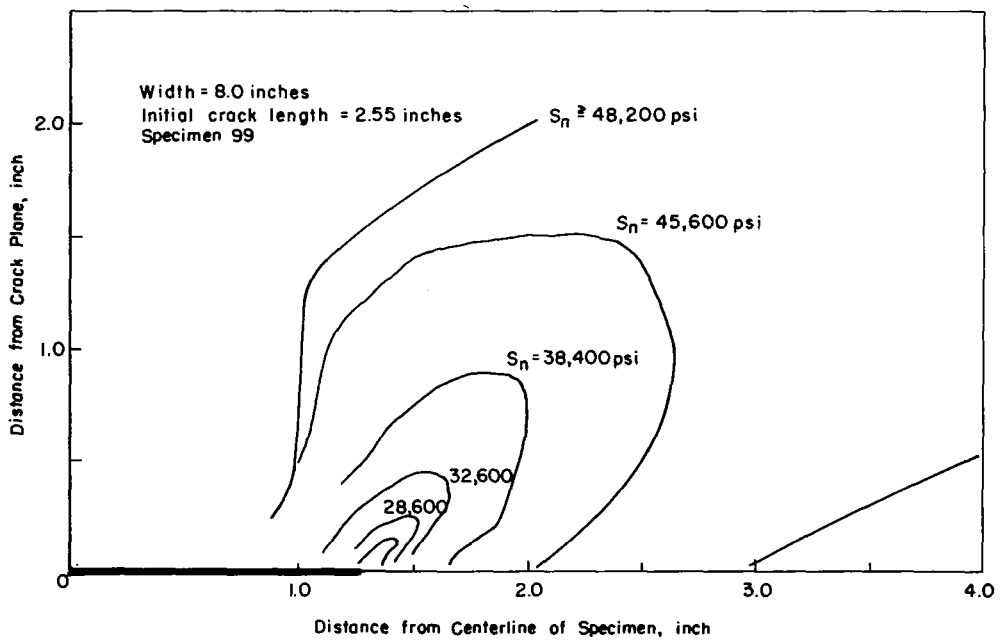

FIGURE 51. PLASTIC ZONE IN 2024-T3, 0.051-INCH-THICK SPECIMEN AS DETERMINED BY PHOTOELASTIC MEANS

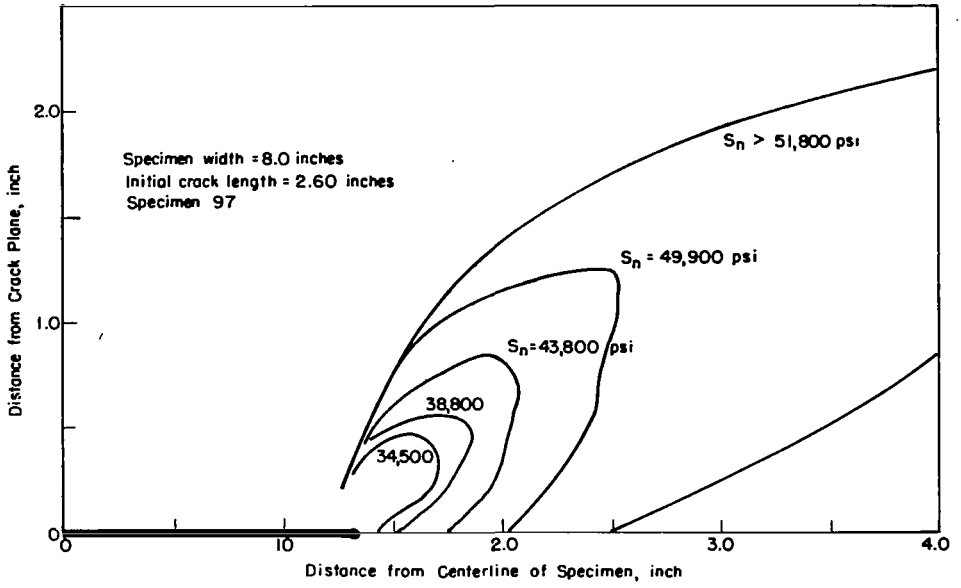

FIGURE 52. PLASTIC ZONE IN 2024-T3, 0.125-INCH-THICK SPECIMEN AS DETERMINED BY PHOTOELASTIC MEANS

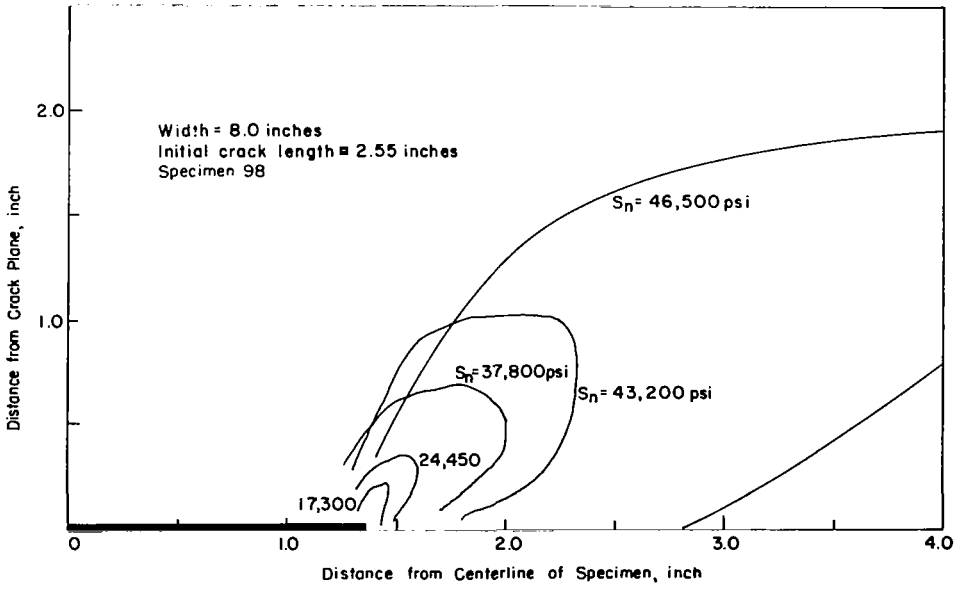

FIGURE 53. PLASTIC ZONE IN 2024-T3, 0.500-INCH-THICK SPECIMEN AS DETERMINED BY PHOTOELASTIC MEANS

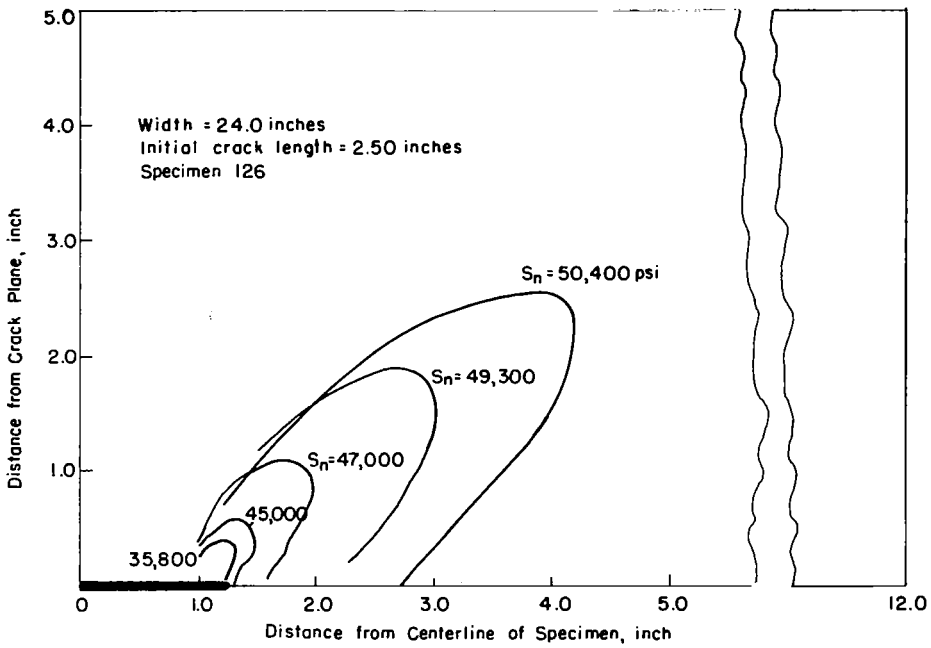

FIGURE 54. PLASTIC ZONE IN 2024-T3, 0.123-INCH-THICK SPECIMEN AS DETERMINED BY PHOTOELASTIC MEANS

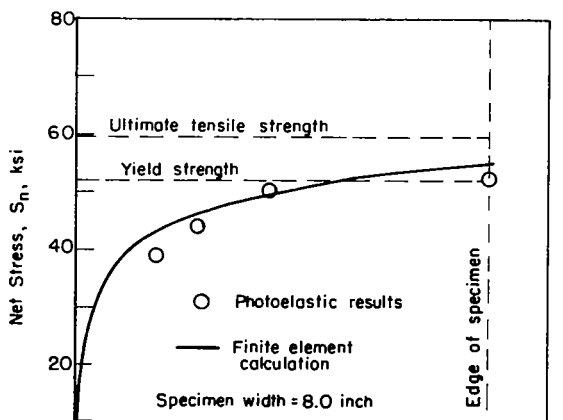

FIGURE 55. PROPAGATION OF PLASTIC ZONE AS MEASURED AT 40-DEGREE ANGLE FROM CRACK TIP (2024-T3, 0.125-INCH-THICK SPECIMEN)

The extent of the plastic zone was determined from the fringe patterns as follows. From the known sensitivity of the coating, the following relation between fringe numbers and principal strain differences were determined.

Fringe 1	$\epsilon_1 - \epsilon_2 = 0.00379$ in./in.
Fringe 2	$\epsilon_1 - \epsilon_2 = 0.00758$ in./in.
Fringe 3	$\epsilon_1 - \epsilon_2 = 0.01137$ in./in.
Fringe 4	$\epsilon_1 - \epsilon_2 = 0.01516$ in./in.

As discussed in Appendix C, yield is indicated when

$$\epsilon_1 - \epsilon_2 \geq \frac{Y(1+\nu)}{E}$$

taking the 0.123-inch-thick material with Y = 52,150 psi, E = 10.6×10^6 psi and $\nu = 1/3$, then

$$\epsilon_1 - \epsilon_2 \geq 0.00656$$

This implies that the yield fringe is

$$\text{Yield Fringe} = \frac{0.00656}{0.00379} = 1.73$$

Location of the 1.73 fringe required interpolation between Fringes 1 and 2.

Comparison of the calculated and measured zones is made in Figure 55. The curve shows the maximum extent of the plastic zone as measured at 40-degree angle from the crack tip. The experimental points were obtained from Figure 52 for the 0.125-inch-thick specimen with crack aspect ratio of 1/3, and the results are in quite good agreement. The differences may be due to a number of factors. Among these are experimental error in the photoelastic measurements, use of the Tresca yield criterion for the experimental work and the von Mises in the calculations, errors in judgement in locating contours between data points, effects of residual stresses on the experimental results, and errors in the assumed values of the elastic constants.

Some general conclusions can be formed on the basis of the above data. The calculated and measured plastic zones are in quite good agreement both as to shape and size. It is clear that for all except perhaps the 24-inch-wide specimens, the plastic zones had grown to the edge of the specimen prior to fracture. The plastic zones in the 0.500-inch-thick specimen were much like those in the 0.050-inch-thick specimen, which indicates that plane-stress conditions governed in both cases.

Interpretation of Crack-Growth Data

The experimental results have been plotted in Figures 56 to 58 for comparison with the results of the elastic-plastic analyses. The experimental data have been separated into groups with respect to plate thickness. For each specimen, three points are plotted and connected by lines to show the stages of crack growth. The three points are defined the same here as in the Engineering Evaluation part of this report. In particular, the first point corresponds to ($2c_o$, S_o) or the threshold of slow crack growth, the second point corresponds to ($2c_1$, S_1) where crack growth accelerates, and the last point corresponds to ($2c_2$, S_1) or the onset of final fracture.

The three curves on Figures 56 to 58 locate the experimental data with respect to the predictions of elastic-plastic analyses. It is of interest to know the load required to produce gross yielding of the plate cross section, since in the absence of brittle fracture this will define the load-carrying capacity of the plate. The three curves are the tensile instability load from the Dugdale analysis of the finite-width plate, the net-yield-stress line of (1-2c/W) times the gross stress, and the consensus of the finite-element and photoelastic-zone determinations.

Although the behavior of all specimens followed essentially the same pattern, some trends with respect to plate width and thickness seem to be evident. The 0.500-inch specimens showed somewhat less slow crack growth than the 0.050 or 0.123-inch thicknesses, although final fracture occurred at about the same applied stress. The width effect reflects the trend of linear-fracture mechanics with the wider specimens fracturing at somewhat lower stresses.

In most simple terms, the fracture process observed for this material in the experimental studies begins when the state of stress is essentially elastic. Then a stage of slow crack growth under increasing load continues until the plate cross section becomes entirely plastic at which time final fracture occurs. As discussed in the Engineering Evaluation section, the threshold of slow growth correlates with stress-intensity factors of linear-fracture mechanics. However, the subsequent slow-crack-growth process is beyond the normal scope of linear-fracture mechanics, since simple elastic-energy considerations predict unstable growth after a critical stress intensity is exceeded. In contrast, the observed growth in the present study was clearly stable in character, since it occurred under conditions of increasing load. In this context, the growth must be considered stable during the stage of growth from length $2c_1$ to $2c_2$. Although in Figures 56 to 58, no increase in load is indicated during this stage, the testing machine maintained constant loading rate. Thus, it is estimated that a few hundred psi increase in gross stress did occur. In terms of net stress, the increase was much greater since the remaining cross-sectional area decreased as the crack grew from length $2c_1$ to $2c_2$.

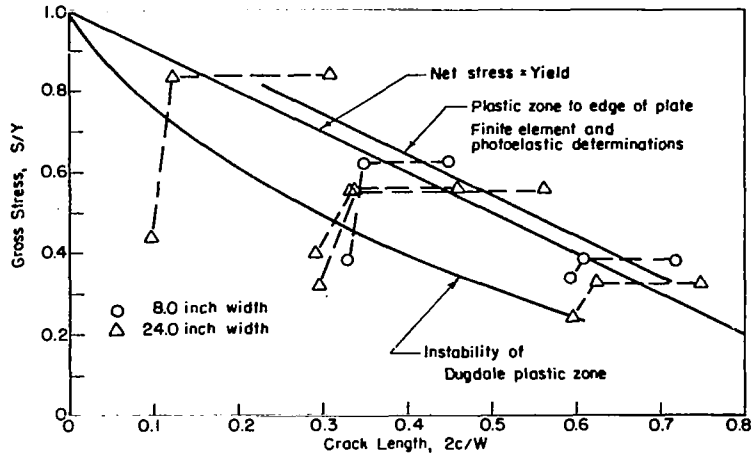

FIGURE 56. CRACK-GROWTH DATA FOR 0.050 INCH THICKNESS RELATED TO CRITERIA FOR GROSS YIELDING OF SPECIMEN

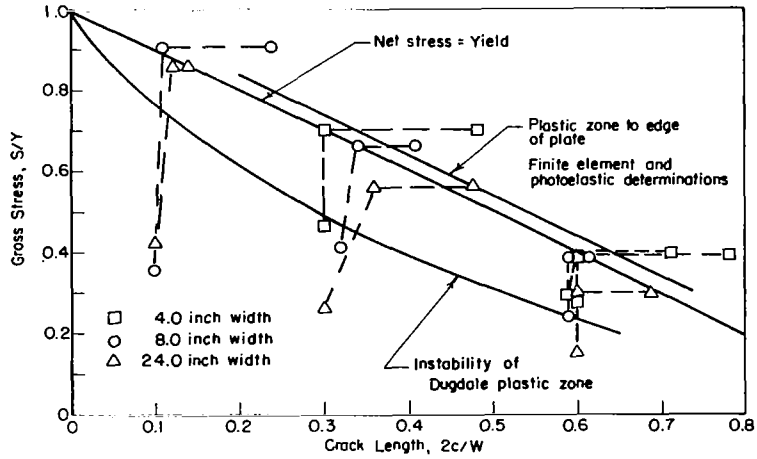

FIGURE 57. CRACK-GROWTH DATA FOR 0.123 INCH THICKNESS RELATED TO CRITERIA FOR GROSS YIELDING OF SPECIMEN

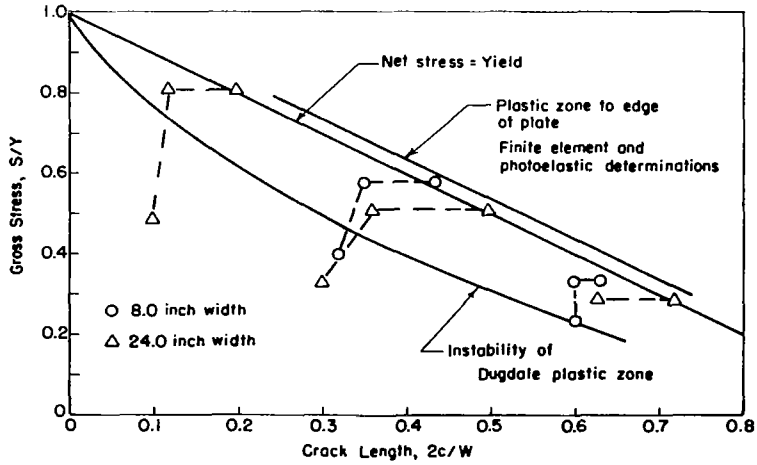

FIGURE 58. CRACK-GROWTH DATA FOR 0.500 INCH THICKNESS RELATED TO CRITERIA FOR GROSS YIELDING OF SPECIMEN

Analysis of the Slow-Crack-Growth Process

The observed stress-crack size combinations (S_1, $2c_2$) corresponding to final fracture (Figures 56 to 58) correlate well with the rapid increase in crack-tip strains associated with gross yielding. However, a complete theoretical picture must also include an analysis of the slow stage of crack growth, so that given the initial flaw size one can predict both final or critical flaw size ($2c_2$) and corresponding maximum load. Due to the complexity of the problem, only brief consideration of such a theory was possible in the present program. The following discussion pertains in a qualitative sense to the factors governing the process of slow crack growth.

Review of McClintock Analysis

The work of McClintock is most relevant to the present program.[2] In his work an analysis was developed which predicted stable crack growth under conditions of transverse shear. In addition, experimental results obtained for H19 temper aluminum foil under biaxial tensile loading were consistent with the theory. In effect, a strain criterion for fracture similar to that of Neuber[10] was employed, whereby, over some fixed distance beyond the crack tip, a critical strain must be exceeded. The distance and strain were taken as material constants. A solution due to Hult[21] for the plastic strains ahead of an extending crack is applied to predict crack growth. This solution gives the strain α for a stationary crack in the form

$$\alpha \sim \frac{1}{r}(\ell/c) \quad , \tag{21}$$

where r is the distance from the crack tip, and ℓ/c is the ratio of plastic-zone size to crack length. Thus the strain and plastic-zone size are directly related.

McClintock's results show the following characteristics:

(1) Of two geometrically similar specimens, the larger will crack at the lower stress. An inverse square root of the crack-length relationship of stress to critical flaw size is predicted, which agrees with linear-fracture mechanics.

(2) The initial crack growth is stable; that is an increase in load is required after the first increment of growth. This results in a stress crack length curve of the type shown in Figure 59.

(3) While there is more slow crack growth for the larger of two geometrically similar specimens, the percent increase in crack length will be less.

(4) Residual stresses develop at the tip of a growing crack due to prior plastic-zone growth, and the existence of stable crack growth is related to these stresses.

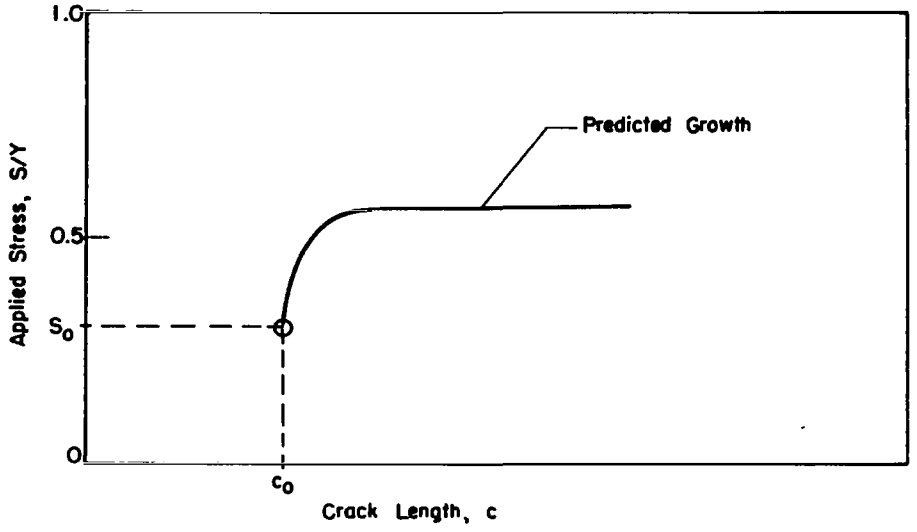

FIGURE 59. STRESS-TO-CRACK-LENGTH RELATIONSHIP PREDICTED BY McCLINTOCK THEORY

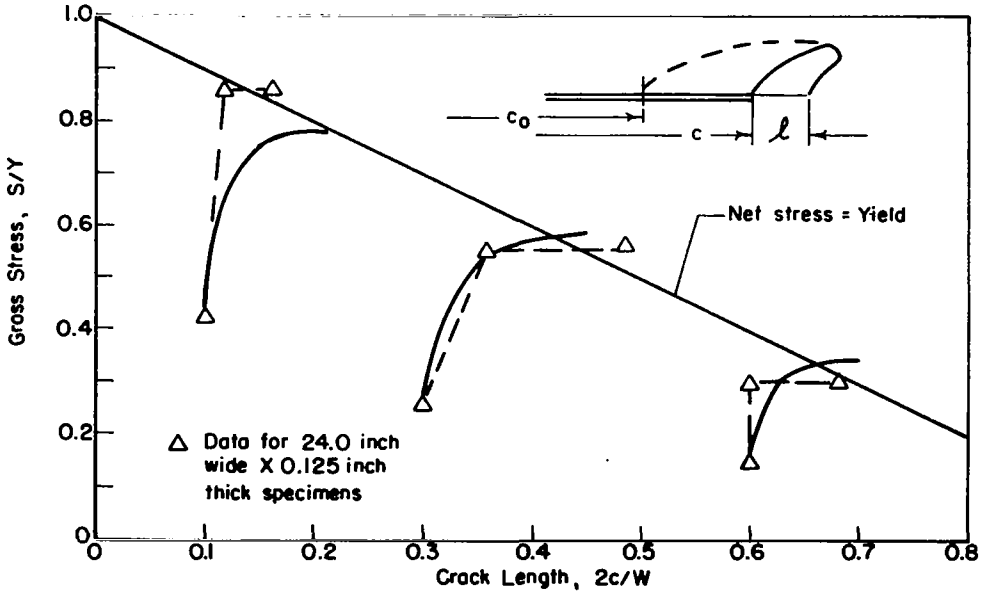

FIGURE 60. PREDICTION OF SLOW CRACK GROWTH ON BASIS OF ELEMENTARY PLASTIC-ZONE-SIZE CONSIDERATIONS

A Simple Crack-Growth Analysis

Predictions of the model developed by McClintock agree generally with the crack-growth data of the present program. In particular, the crack-length-versus-stress curves show the same behavior, and the predicted effects of plate size are correct. On the other hand, since the solutions are for an infinite region, no effects of aspect ratio are predicted.

Unfortunately, explicit solutions of the type used by McClintock are not available for the loadings and geometries of the present program. However, it is easy to show that load-crack length curves of the proper form can be constructed on the basis of the available plastic-zone-size data. For example, one might assume that crack growth begins at a stress S_o for an initial crack length $2c_o$ and that S_o can be calculated on the basis of a critical stress-intensity factor. Going one step further, assume that the crack grows in such a manner that

$$n(c - c_o)/c = (\ell - \ell_o)/c \quad , \tag{22}$$

where n is a proportionality factor, and ℓ_o is the plastic-zone size corresponding to S_o. This implies that the strain at the crack tip is proportional to the plastic-zone size, and that the residual stress due to prior plastic deformation is related to the amount of prior crack growth,

$$\ell/c = 0.03 \left(1 - \frac{2c}{W}\right)^2 \exp\left[\frac{4.14}{1 - \frac{2c}{W}} S/Y\right] \quad , \tag{23}$$

gave a reasonable representation of the calculated and measured plastic-zone sizes. Combining this with the assumed crack-growth relation gives

$$S/Y = \frac{1}{4.14}\left(1 - \frac{2c}{W}\right) \ln\left[\frac{\ell_{o/c} + n\,(1 - c_{o/c})}{.03\,(1 - 2c/w)}\right] \quad , \tag{24}$$

which allows prediction of a load crack length behavior for $S > S_o$. This has been applied to the 0.123-inch-thick specimens for the 24-inch width, taking n = 2.0. The results are shown on Figure 60, and qualitative agreement with the experimental slow-crack-growth data was obtained.

The heuristic nature of the analysis does not warrant further calculations. It is significant however, that simple plastic-zone-size considerations give rise to the proper type of crack-growth curve, with a low rate of growth initially followed by a rapidly accelerating growth rate. In addition a picture of the fundamental physical process involved in slow crack growth can be proposed. It is a stable process, with the plastic-strain fields left by the growing crack acting to arrest growth until an increase in applied load allows further growth.

CONCLUDING REMARKS

On this program, a study of plane-stress and transitional-stress state fracture behavior of 2024-T3 and -T351 aluminum alloy sheet and plate in thicknesses through 1/2 inch and in panel widths through 24 inches was made. Of primary interest were the parametric effects of thickness, width, and plasticity which were analyzed from both a practical-engineering perspective and a more-rigorous theoretical perspective. Complementary efforts in the identification of the onset of slow growth, the identification of rapid fracture, and the experimental determination of the plastic-zone size were included.

In the rising-load fracture test of a center-cracked tension panel, specimen response begins in a linear and elastic fashion. At some level of stress, dependent on crack size, material characteristics, and panel geometry, nonlinearity in specimen response is detectable due to a slow, stable growth of the crack and/or crack-tip plasticity. Although precise discrimination between crack growth and plasticity effects is difficult, useful engineering estimates was accomplished by visual or photographic observations, and graphical offsets on the load records. This threshold or onset of slow growth was identified by the crack size-stress level coordinate pair $(2c_o, S_o)$. This is an important benchmark in the rising-load test since it represents an increase in the macroscopic physical-damage state of the specimen.

As further loading was applied, slow, stable crack growth continues until instability was manifested as a sudden acceleration pulse. On photographic records, it was noted that the slow growth proceeded at a nearly uniform velocity (generally, a small fraction of an inch per second) to a crack length, $2c_1$. Here a sudden and brief acceleration pulse dramatically changed the crack velocity. At a crack length of $2c_2$, a high, nearly constant terminal velocity (>>1 inch/second) was achieved which carried the crack to the boundary. The critical crack length is considered to be bracketed by the measurements $2c_1$ and $2c_2$. While this is not a precise length, it appears to be a reasonable engineering estimate. Since the time differential (less than one second) associated with this crack-length increment was small, and since the loading rate was low, the associated maximum-stress level is nearly constant. Therefore, the coordinate pairs $(2c_1, S_1)$ and $(2c_2, S_1)$ are considered to represent the critical condition.

Throughout this process, there was a subtle but intimate relationship between plasticity and slow growth. Plasticity tended to relax the severity of the stress field adjacent to the crack tip, thus permitting the subcritical process of slow growth to predominate overall elastic instability. If this plasticity or "forgiveness" within the material was inhibited, the slow-growth processes would probably reach instability sooner. Thus, thickness and width increases, which provide dimensional restraint on plastic-zone development, tended to increase the crack sensitivity of the material. It is additionally important to recognize that plasticity, while constrained by geometry, is also an intrinsic metallurgical characteristic which may vary from material to material. This means that the conceptual thickness and/or width effects described may be totally masked over or may be compensated by the inherent plasticity or ductility of the material. Of course, it is the function of testing to ferret out the primary characteristics of this behavior.

The results of this program have indicated negligible thickness effects in the fracture behavior of 2024-T3 and -T351 aluminum alloy sheet and plate through thicknesses up to 1/2 inch. Furthermore, no apparent trends toward increased frangibility can be projected for greater thicknesses on the basis of these data. However, there are some

notable width effects relative to the critical fracture conditions. For all thicknesses and in widths through 8 inches, net section yielding appeared to be a real failure characteristic. In the 24-inch widths, for all thicknesses, there was a distinct elastic characteristic for the end of slow growth, or the onset of critical instability, i.e., the coordinate points ($2c_1$, S_1). The significance of this is that the 24-inch-wide panel is a minimum requirement for studying elastic-fracture conditions in 2024-T3 and -T351 sheet and plate. In fact, it suggests that distinctly larger panels, probably 36 inches wide, are needed to study the phenomenon if it is of interest. Relative to the threshold conditions, it is significant that slow growth initiated well within the elastic range (i.e., well below net section yielding). Data scatter coupled with experimental uncertainties in threshold determination suggested no distinct thickness and width effects.

The engineering evaluation of fracture-analysis methods pointed out the variety of concepts utilized to describe fracture behavior. Most of these fall into one of two categories. Either they strive intently toward characterization of all aspects of the material per se, such as the extensive corrections introduced on the stress-intensity factor; or, at the opposite extreme, they apply creative but intuitive techniques of analytical modeling which result in pseudoparameters of material behavior such as the effective-width techniques or notch-strength analysis. A bridging across the gap at the materials-structures interface is needed to marry the two technologies. Such a technique has been proposed and is illustrated within this report. Both threshold of slow growth and critical fracture stability can be presented on a common format. Their relationship can be visually compared or even reduced to the more elementary notch-strength format. Its power lies in satisfying the dual function of a function of a fracture index: (1) it must provide a qualitative rating of fracture resistance for materials-selection purposes, and (2) it must be quantifiable for engineering design. While the concept is not new, the method is new. The resultant interpretations which may be derived from this method are believed to be quite powerful for elucidating flaw-growth behavior.

The theoretical analysis was undertaken to establish the elastic-plastic criteria associated with plane-stress fracture. Although a definitive strain criterion did not evolve, significant insight was gained to the manifestation of tensile instability. The Dugdale model was demonstrated to be inadequate for this structural material because of the two-dimensionality in plastic-zone development. However, finite-element techniques were quite useful in predicting the size and shape of the plastic zones. Photoelastic analysis correlated analytical procedures very well and demonstrated the power of the finite-element procedure.

References

(1) Brown, W. F., Jr., and Srawley, J. E., "Plane Strain Crack Toughness Testing of High Strength Metallic Materials", Am. Soc. Testing Mater., STP No. 410 (1966).

(2) McClintock, F. A., "Ductile Fracture Instability in Shear", J. Appl. Mech., 80 (2), 582-588 (December, 1958).

(3) Broek, D., de Rijk, P., Sevehuysen, "The Transition of Fatigue Cracks in Alclad, NLR 2100", National Luchten Ruimtevaart Laboratorium, Amsterdam, Holland, August, 1965.

(4) Griffith, A. A., "The Phenomena of Rupture and Flow in Solids", Trans. Roy. Soc. (London), 221, p 163-198 (1920).

(5) Irwin, G. R., "Fracture", Handbuch Der Physik, Vol VI, Springer, Berlin (1958).

(6) Irwin, G. R., "Analysis of Stresses and Strains Near the End of a Crack Traversing a Plate", J. Appl. Mech., 21, 361-364 (1957).

(7) Westergaard, H. M., "Bearing Pressures and Cracks", Trans. ASME, 61, A49-A53 (1939).

(8) Crichlow, W. J., "The Ultimate Strength of Damaged Structure-Analysis Methods With Correlating Test Data", in Full Scale Fatigue Testing of Aircraft Structures, Proceedings of the Symposium held in Amsterdam, June, 1959, Pergamon Press (1961), pp 149-209.

(9) Christensen, R. H., and Denke, P. H., "Crack Strength and Crack Propagation Characteristics of High Strength Metals", ASD-TR-61-207, May, 1961, Douglas Aircraft Company.

(10) Neuber, H., Theory of Notch Stresses: Principles for Exact Stress Calculation, J. W. Edwards, Ann Arbor, Michigan (1946).

(11) Kuhn, Paul, and Figge, I. E., "Unified Notch-Strength Analysis for Wrought Aluminum Alloys", NASA TD-D-1259 (1962).

(12) Dixon, J. R., "Stress Distribution Around a Central Crack in a Plate Loaded in Tension; Effect of Finite Width of Plate", J. Roy. Aero. Soc., 64, pp 141-145 (1960).

(13) Kuhn, Paul, "Residual Strength in the Presence of Fatigue Cracks", Presentation to the AGARD Structures and Materials Panel, 1967.

(14) Hudson, C. Michael, "Effect of Stress Ratio on Fatigue-Crack Growth in 7075-T6 and 2024-T3 Aluminum Alloy Specimens", NASA TN-D-5390 (August, 1969).

(15) Fracture and Fatigue Crack Propagation Characteristics of 7075-T7351 Aluminum Alloy Sheet and Plate, Contract No. N00156-68-C-1345 with Naval Air Engineering Center, Philadelphia, Pa. (to be published).

(16) Eichenburger, T. W., "Fracture Resistance Data Summary", Boeing Airplane Report No. D2-20947 (June, 1962).

(17) Orange, T. W., "Fracture Toughness of Wide 2014-T6 Aluminum Sheet at -320 F", NASA TN-D-4017 (June, 1967).

(18) Hulbert, L. E., Hahn, G. T., Rosenfield, A. R., and Kanninen, M. F., "An Elastic-Plastic Analysis of a Crack in a Plate of Finite Size", presented at the 12th International Congress of Applied Mechanics, Stanford, California, August 26-31, 1968.

(19) Swedlow, J. L., Williams, M. L., and Yang, W. H., "Elasto-Plastic Stresses and Strains in Cracked Plates", Proceedings of the First International Conference on Fracture, Vol 1, Sendai, Japan (September, 1965).

(20) Marcal, P. V., and King, I. P., "Elastic-Plastic Analysis of Two Dimensional Stress Systems by the Finite Element Method", Int. J. Mech. Sci., 9, 143-155 (1967).

(21) Hult, J. A. H., "Fatigue Crack Propagation in Torsion", J. Mech. Phys. Solids, 6, 47-52 (1957).

APPENDIX A

PRELIMINARY FRACTURE TESTS

For the preliminary tests, the following thicknesses (in inches) of bare 2024-T3 and T-351 were tested: 0.020, 0.032, 0.040, 0.050, 0.063, 0.125, 0.190, 0.250, 0.3125, 0.375, 0.500, 0.625 and 0.750. These thicknesses were selected on the basis of the belief that they would provide meaningful data on the fracture behavior of the base 2024 alloy in the plane stress and transition region.

Prior to making the fracture tests, tensile tests were conducted to verify typical mechanical properties for the alloy. Two tensile tests were conducted for each thickness, except the 0.625- and 0.750-inch-thick material using standard tensile-test procedures. The results are summarized in Table A-1. They show the material to be typical of this alloy and heat treatment, except for the 3/8-inch-thick material. For this thickness, the yield strength was slightly below the MIL-HDBK-5A value.

For all thicknesses cited above, three fracture tests were conducted. For thicknesses through 0.3125 inch and for 0.500-inch thick specimens some tests were performed with and without buckling guides. For 0.375-, 0.625- and 0.750-inch-thick specimens, no buckling guides were used. This procedure was followed to ascertain if the use of buckling guides had any discernible effect on the residual static strength of precracked 2024.

The specimen was 8 inches wide by 32 inches long. The gripping pattern varied depending on thickness since different test systems were employed to conduct the tests. The starter flaw consisted of a centrally drilled and reamed 1/4-inch-diameter hole extended by electric-discharge machining. Prior to fracture testing, the EDM slot was saw-cut along the specimen midplane to a total crack length of 1.8 inches. Since the crack length desired for the fracture test was approximately 2.6 inches, the last 0.8 inch of crack was introduced by fatigue loading. All fatigue cracking was performed such that the resultant crack was flat and such that the final stress-intensity level of fatigue cracking was the same for all specimens.

The tests were conducted in 25-kip, 50-kip, and 170-kip maximum static-load capacity electrohydraulic servocontrolled test systems using load control. After precracking, a compliance gage was inserted into the centrally drilled hole for measurement of crack-opening displacement (COD) during the fracture test. The compliance gage is a double-cantilever clip type, constructed from 17-7 PH stainless steel with a bridge of four active gages. Calibration curves were constructed giving bridge output as a function of gage displacement.

As previously mentioned, buckling guides were used on some tests. These guides consisted of 1/4-inch-thick steel plates lined with wax paper on the face contacting the specimens. A hole was drilled in one of the buckling guides through which the compliance gage was inserted. The other buckling guide possessed a slot machined along its width about 1/4 inch on each side of the crack plane to permit viewing the progress of the crack during the course of the test. During each test, movies of the slow-crack-growth phase were taken at 128 frames per second. This was done to permit the

TABLE A-1. VERIFICATION-TEST DATA FOR TENSILE PROPERTIES OF 2024-T3 ALUMINUM ALLOY

Specimen	Thickness, inch	0.2 Percent Yield Strength, psi	Ultimate Tensile Strength, psi	Elongation, percent in 2 inches
1	0.020	53,500	68,500	17.0
2	0.020	47,500	68,500	18.0
Average		50,500	68,500	17.5
1	0.032	50,900	70,500	18.0
2	0.032	50,600	70,500	17.5
Average		50,750	70,500	17.75
1	0.040	47,700	66,300	18.0
2	0.040	48,300	66,800	20.5
Average		48,000	66,550	19.25
1	0.0512	50,200	68,900	19.5
2	0.0512	49,900	68,800	19.5
Average		50,050	68,850	19.5
1	0.065	53,100	74,200	20.8
2	0.065	52,500	74,200	20.0
Average		52,800	74,200	20.4
1	0.125	52,000	69,400	17.5
2	0.125	52,300	69,500	18.5
Average		52,150	69,450	18.0
1	0.1855	51,200	69,000	19.0
2	0.1855	51,400	70,000	20.5
Average		51,300	69,500	19.75
1	0.2593	55,200	71,500	20.0
2	0.2593	55,100	71,800	18.0
Average		55,150	71,650	19.0
1	0.3124	54,800	69,900	22.0
2	0.3124	55,100	70,200	20.0
Average		54,950	70,050	21.0
1	0.381	45,200	67,700	22.0
2	0.381	45,200	67,800	22.0
Average		45,200	67,750	22.0
1	0.505	52,800	67,200	22.0
2	0.505	52,800	67,100	21.0
Average		52,800	67,150	21.5
1	0.629	55,600	71,100	21.0
2	0.760	53,900	69,600	19.5

determination of the critical crack length ($2c_c$), as the crack length immediately prior to fracture on the film record. (It should be noted that $2c_c$ is different from 2c, and $2c_2$ crack length designations in the report.)

The preliminary fracture tests were conducted at a loading rate that produced an initial elastic strain rate of 0.005 in./in./min. Constant load rate was used to prevent drop-off in load when pop-in occurred. The compliance gage output was the X-axis input to an X-Y recorder, with the Y axis recording the load level. Thus, the record of each test consists of a load-COD plot, a movie of the crack growth, and the fracture surface.

There are various ways to present and review the data. In this Appendix several of these methods are presented as described below:

(1) Gross fracture stress, S_g, computed from the maximum test load, P_{max}, and the gross area of the specimen, $A_g = BW$ (B = thickness, W = width).

(2) Net fracture stress, S_n, computed from the maximum test load, P_{max}, and the net area of the specimen based on the original crack length, $2c_o$.

(3) The stress intensity factor, $K_{app_{co}}$, based upon the gross fracture stress, S_g, the original crack length, $2c_o$, and a width correction factor[1]

$$K_{app_{co}} = S_g\sqrt{\pi\, c_o \sec\left(\frac{\pi c_o}{w}\right)} \quad . \tag{A-1}$$

(4) The stress intensity factor K_c based upon the gross fracture stress, S_g, the critical crack length, $2C_c$ and a width correction factor

$$K_c = S_g\sqrt{\pi\, c_c \sec\left(\frac{\pi c_c}{w}\right)} \quad . \tag{A-2}$$

(5) The net fracture stress, S_n, computed from the maximum test load, P_{max}, and the net area of the specimen based on the critical crack length $2c_c$.

The above techniques provide a variety of analytical perspectives to evaluate the thickness effect and to examine various parametric influences on the data.

Table A-2 contains a summary of the results of all of the fracture tests as well as the summary of computations described in Items (1), (2), and (3) above for gross fracture stress, net fracture stress and the stress-intensity factor, $Kapp_{co}$, respectively. The results listed in Table A-2 are plotted in Figures A-1, A-2, and A-3 as gross stress versus thickness, net stress versus thickness, and stress intensity versus thickness, respectively. The open circles on these figures represent the results with buckling guides, while the solid circles represent the results without buckling guides.

TABLE A-2. FRACTURE TEST RESULTS

Specimen	Thickness, in.	Width, in.	Gross Area, sq. in.	Crack Length, in.		Gross Fracture Stress,	Net Fracture Stress,	Stress Intensity Factor, ksi$\sqrt{\text{in.}}$
				Initial $2c_o$	Critical $2c_c$	S_g, ksi	S_n, ksi	$K_{app_{co}}$
2 G[a]	0.020	8.010	0.1602	2.70		29.960	45.200	67.115
3 G	0.0195	8.050	0.157	2.62	4.65	33.100	49.200	69.750
4	0.0195	8.010	0.1561	2.60	4.56	26.500	37.900	57.500
38	0.032	8.000	0.256	2.57	4.60	28.320	41.715	60.739
39 G	0.033	8.000	0.264	2.50	4.40	34.091	49.587	71.754
40 G	0.032	8.010	0.2563	2.52	4.30	33.359	48.662	70.721
34	0.041	8.010	0.3284	2.54	4.63	29.689	43.468	63.237
35 G[b]	0.041	8.000	0.328	2.49	4.50	30.259	43.935	63.543
36 G[b]	0.041	8.000	0.328	2.53	4.65	29.344	42.911	62.356
37 G	0.041	8.000	0.328	2.52		32.012	46.729	67.865
31	0.051	8.010	0.4085	2.52	4.40	30.477	44.464	64.611
32 G	0.053	8.010	0.4245	2.50	4.53	31.802	46.233	67.102
33 G	0.051	8.000	0.4080	2.60	4.60	32.414	48.021	70.04
1 G	0.065	8.005	0.520	2.55	3.24	33.650	49.350	67.980
5 G	0.065	8.010	0.5207	2.67	3.25	33.100	51.400	73.000
30 G	0.066	8.000	0.528	2.55	3.60	33.428	49.068	71.369
26 G	0.125	8.010	1.001	2.60	4.80	33.766	50.000	72.935
27 G	0.123	8.020	0.9864	2.57	3.70	34.570	50.872	73.979
28	0.125	8.010	1.001	2.58	4.90	33.067	48.784	71.755
20 G	0.187	8.005	1.496	2.63	3.15	32.286	48.107	70.300
21 G	0.187	8.005	1.480	2.63	2.90	32.230	48.381	70.261
22	0.187	8.002	1.496	2.64	2.90	32.560	48.602	70.980
23 G	0.260	8.006	2.081	2.67	3.64	32.388	48.600	71.254
24 G	0.261	8.003	2.088	2.65	3.60	30.555	45.702	67.800
25	0.260	8.003	2.080	2.594	3.50	32.260	47.700	69.500
17 G	0.310	8.003	2.481	2.672	3.15	30.935	46.430	69.450
18 G	0.312	8.007	2.498	2.610	2.82	32.120	47.600	69.600
19	0.309	8.005	2.479	2.810	3.35	30.900	47.548	70.100
15	0.380	7.810	2.967	2.70	3.35	31.344	47.913	69.520

TABLE A-2. (Continued)

Specimen	Thickness, in.	Width, in.	Gross Area, sq. in.	Crack Length, in.		Gross Fracture Stress, S_g, ksi	Net Fracture Stress, S_n, ksi	Stress Intensity Factor, ksi$\sqrt{\text{in.}}$ $K_{app_{co}}$
				Initial $2c_o$	Critical $2c_c$			
16	0.376	7.800	2.932	2.82	3.36	31.036	48.611	70.762
6 G	0.504	8.001	4.032	2.55	3.10	31.498	46.232	67.248
7 G	0.506	8.007	4.051	2.66	3.35	31.103	46.580	68.271
8	0.503	8.001	4.024	2.67	3.10	31.262	46.922	68.770
12	0.626	8.005	5.011	2.656	2.70	31.131	46.595	68.177
13	0.629	8.003	5.033	2.560	3.20	31.393	46.158	67.181
14	0.629	8.003	5.033	2.68	3.10	31.393	47.206	69.055
9	0.760	8.000	6.080	2.67	3.20	29.934	44.927	65.846
10	0.760	7.980	6.064	2.57	3.00	30.672	45.244	65.900
11	0.760	8.006	6.084	2.78	2.80	30.900	47.343	69.834

(a) The letter G after the specimen number indicates buckling guides were used.
(b) Data may be questionable. Specimen buckled slightly before fracture.

In Figures A-1 and A-2 the data from specimens with buckling guides suggest that gross and net section stress (based on the original crack length) increases slightly as specimen thickness increases to a maximum value at a thickness of about 1/8 inch, and gradually decreases over the remaining thickness range (up to 3/4 inch). The data also suggest that for thicknesses greater than about 3/16 inch, there is no difference in results if guide plates are used or not. Finally, the two figures clearly show that for thicknesses less than 3/16 inch, the lack of guide plates results in a lowering of the strength of the panels. Figure A-3, concerned with stress intensity factor as a function of thickness, shows essentially the same features. However it is interesting that the spread between the maximum value at about B = 1/8 inch and the value at B = 3/4 inch is as small as it is. Since the K values appear to be decreasing at a thickness of 0.75 inch, it is probable that the minimum K value has not been achieved. It is of interest to note in all three figures that the basic data illustrate little scatter.

Other formulations that have been used to evaluate fracture data employ the critical crack length at failure and the maximum load. Items 4 and 5 described previously involve either the net section stress or a stress intensity, K_c. Table A-3 and Figure A-4 contain a summary of the pertinent information.

The various formulations illustrated show for 2024-T3 sheet and plate (T351) that there is some evidence of a slight thickness effect in thicknesses up to about 1/4 inch. The magnitude of this effect varies with the measure. As a matter of fact, a greater effect than was observed was expected, as pointed out previously. However, all of the failures for this width specimen and crack aspect ratio were at net section yield stress or greater, which would be expected to minimize this effect.

The nature of the fracture surfaces also showed real differences as thickness increased. With the exception of the 5/8-inch and 3/4-inch gages, all fracture surfaces showed flat, transition and full or nearly full slant fractures to some degree. Three approximate groupings can be identified within which the details vary somewhat from specimen to specimen and thickness to thickness:

(1) From 0.020 to 0.125-inch thickness: Flat fracture adjacent to starter-crack tip, changing to transition fracture at least 1/8 inch from the crack tips and becoming full slant fracture 5/8 inch from crack tips.

(2) From 0.188 to 0.500-inch thickness: Flat fracture to about 5/8 inch, transition fracture to about 2-1/8 inches, full slant from 2-1/8 inches to specimen edge.

(3) From 0.625 to 0.750-inch thickness: Flat fracture to almost 1-5/8 inches, slightly transitional beyond 1-5/8 inches (about 20 percent slant fracture).

The first grouping (0.020 to 0.125) corresponds approximately to the region of the stress- or K-thickness graphs where the stress or K value is increasing. The next two groupings (>0.125) correspond to the region of the graphs where stress or K values decrease. As such, there is an implied correlation between fracture appearance and strength.

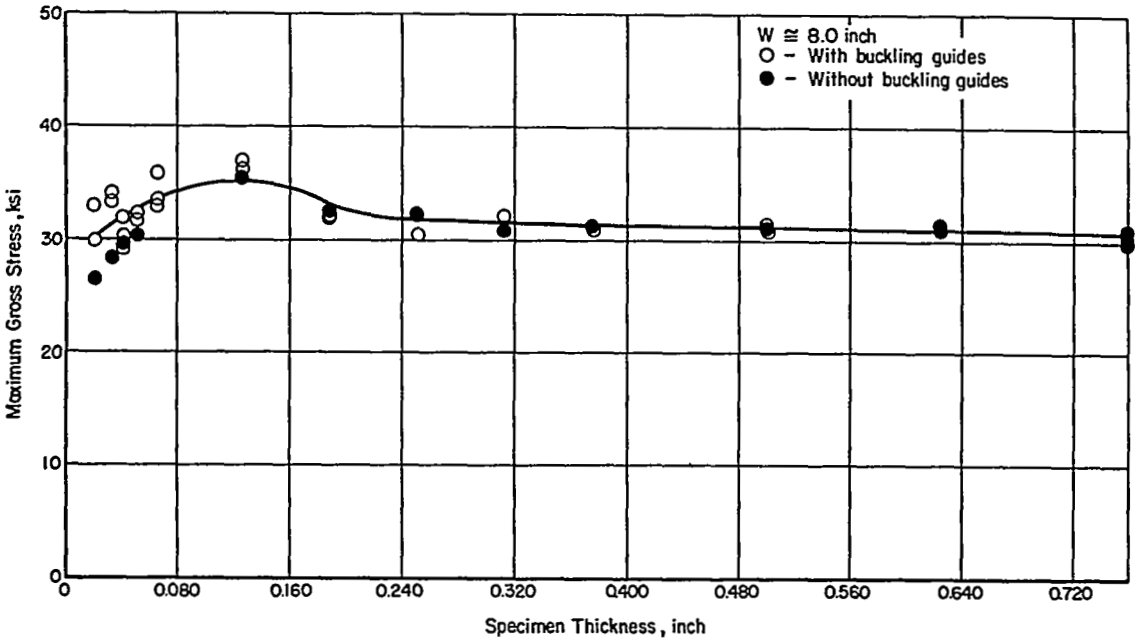

FIGURE A-1. MAXIMUM GROSS STRESS VERSUS SPECIMEN THICKNESS FOR BARE 2024-T3 PRECRACKED TO APPROXIMATELY 2.60 INCHES

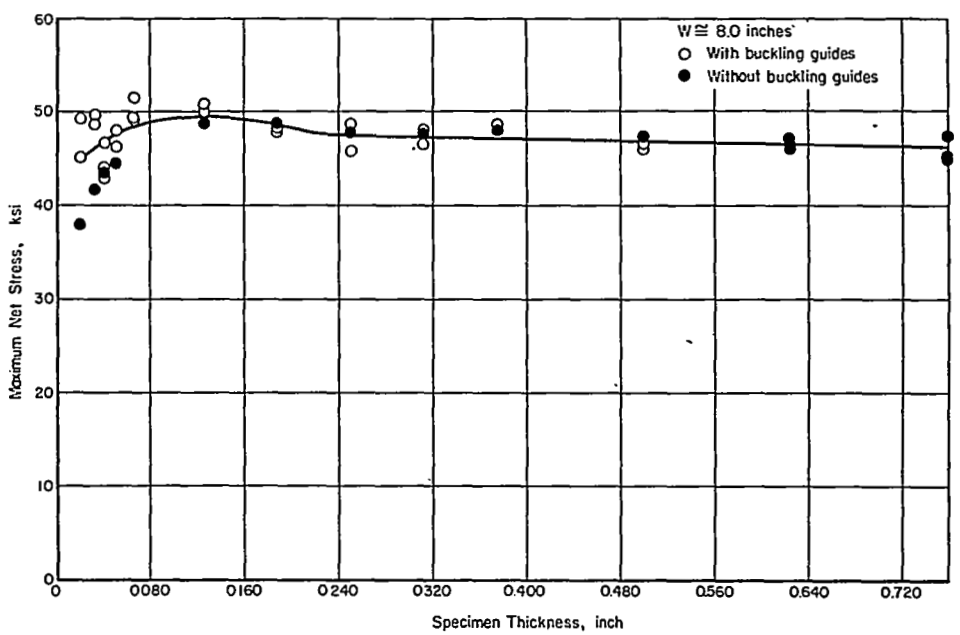

FIGURE A-2. MAXIMUM NET STRESS VERSUS SPECIMEN THICKNESS FOR BARE 2024-T3 PRECRACKED TO APPROXIMATELY 2.6 INCHES (W/3)

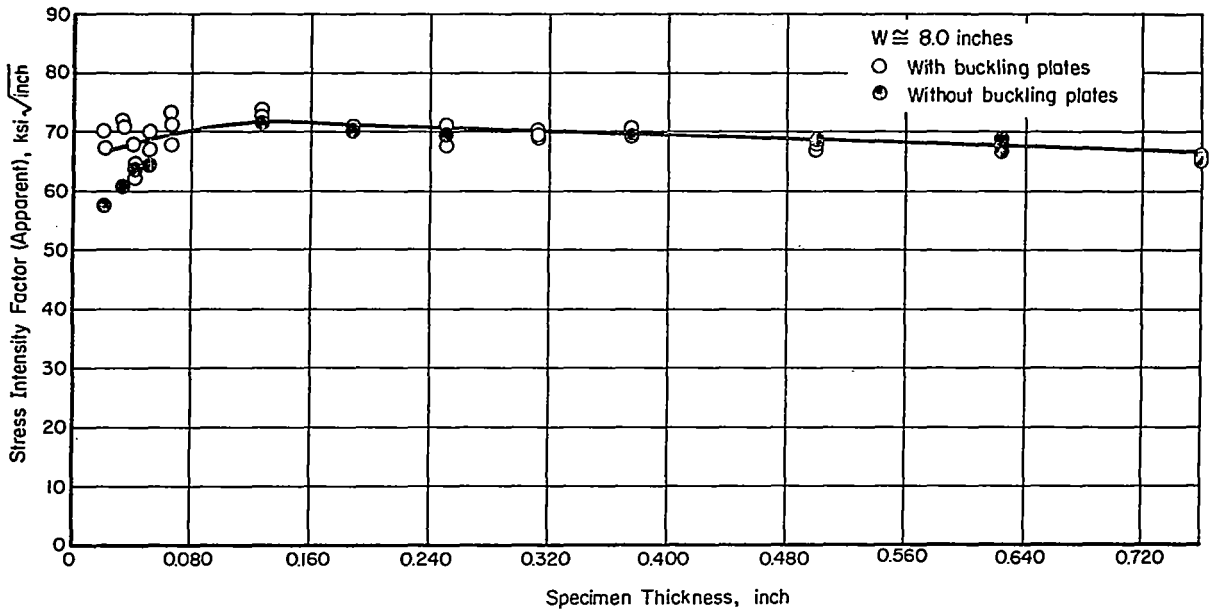

FIGURE A-3. STRESS-INTENSITY FACTOR VERSUS THICKNESS FOR BARE 2024-T3 PRECRACKED TO APPROXIMATELY 2.6 INCHES (W/3)

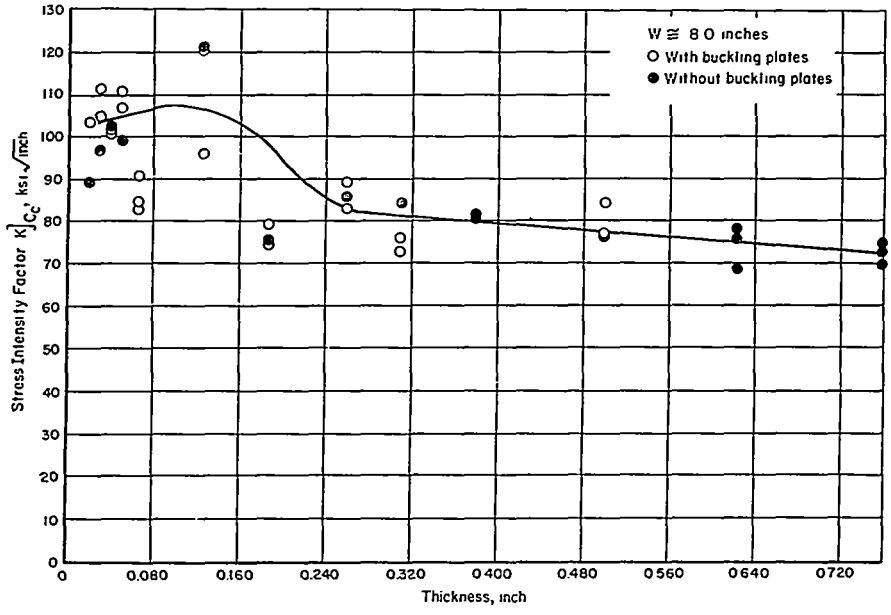

FIGURE A-4. STRESS-INTENSITY FACTOR BASED ON CRITICAL CRACK LENGTH VERSUS THICKNESS FOR BARE 2024-T3

TABLE A-3. NET FRACTURE STRESS AND STRESS INTENSITY BASED UPON CRITICAL CRACK LENGTH

Specimen	Critical Crack Length, $2c_c$, in.	Net Section Stress, S_{n_c}, ksi	Stress Intensity Factor, K_c, ksi$\sqrt{\text{in.}}$
3 G[a]	4.65	78.431	103.486
4	4.56	59.453	89.632
38	4.60	66.636	96.760
39 G	4.40	78.125	111.221
40 G	4.30	72.030	104.886
34	4.63	70.346	102.073
35 G	4.50	69.164	101.015
36 G	4.65	70.488	101.431
31	4.40	67.626	99.369
32 G	4.53	73.210	106.831
33 G	4.60	76.269	110.748
1 G	3.24	56.506	84.631
5 G	3.25	55.753	83.422
30 G	3.60	60.778	91.160
26 G	4.80	84.226	120.842
27 G	3.70	64.170	96.318
28	4.90	85.134	121.225
20 G	3.15	53.200	79.557
21 G	2.90	49.969	74.945
22	2.90	51.043	75.717
23 G	3.64	59.383	89.096
24 G	3.60	55.517	83.320
25	3.50	57.311	86.029
17 G	3.15	51.017	76.228
18 G	2.82	49.620	73.293
19	3.35	53.254	84.026
15	3.35	54.874	81.338
16	3.36	54.511	80.754
6 G	3.10	51.417	76.734
7 G	3.35	53.471	84.573
8	3.10	51.030	76.159
12	2.70	46.975	69.016
13	3.20	52.299	78.250
14	3.10	51.232	76.474
9	3.20	49.890	74.618
10	3.00	49.144	73.055
11	2.80	47.516	70.172

(a) The letter G after the specimen number indicates buckling guides were used.

APPENDIX B

FRACTURE-TOUGHNESS INDICES

Individual values of fracture-toughness which have been used in this report are tabulated in Tables B-1 through B-3. These include both stress-intensity factors (SIF) and crack-sensitivity values. The values are identified by thickness, specimen number, and panel width.

TABLE B-1. FRACTURE-TOUGHNESS INDICES FOR 0.050-INCH-THICK 2024-T3 ALUMINUM ALLOY

Specimen	Nominal Width, W, in.	5 Percent Secant Offset SIF, K_3, ksi-in.$^{1/2}$	Max. Load SIF, K_1, ksi-in.$^{1/2}$	Crack Sensitivity, C_m, in.$^{-1/2}$
99	8.0	42.7	74.9	0.643
102	8.0	63.1	74.1	0.648
				Average C_m 0.646
121	24.0	71.2	108.7	0.603
122	24.0	--	113.6	0.556
123	24.0	77.1	111.8	0.562
124	24.0	43.1	98.2	0.543
				Average C_m 0.564

TABLE B-2. FRACTURE TOUGHNESS INDICES FOR 1/8-INCH THICK 2024-T3 ALUMINUM ALLOY

Specimen	Nominal Width, W, in.	5 Percent Secant Offset SIF K_3, ksi-in.$^{1/2}$	Max. Load SIF, K_1, ksi-in.$^{1/2}$	Crack Sensitivity, C_m, in.$^{-1/2}$
111	4	--	--	--
112	4	36.3	54.7	0.781
113	4	26.1	44.1	1.013
114	4	37.8	54.0	0.758
115	4	31.8	54.9	1.379
116	4	35.6	55.4	0.652
			Average C_m	0.917
97	8	46.3	81.4	0.505
103	8	20.8	57.8	0.681
104	8	--	56.0	0.681
105	8	45.2	73.4	0.611
106	8	51.4	72.5	0.629
			Average C_m	0.621
125	24	--	114.5	0.568
126	24	44.3	101.5	0.450
127	24	44.3	101.0	0.467
128	24	48.4	121.6	0.520
129	24	--	90.1	0.887
130	24	48.5	97.9	0.648
			Average C_m	0.590

TABLE B-3. FRACTURE-TOUGHNESS INDICES FOR 1/2-INCH-THICK 2024-T3 ALUMINUM ALLOY PLATE

Specimen	Nominal Width W, in.	5 Percent Secant Offset SIF K_3, ksi-in.$^{1/2}$	Max. Load SIF, K_1, ksi-in.$^{1/2}$	Crack Sensitivity, C_m, in.$^{-1/2}$
98	8	46.3	72.1	0.705
107	8	50.4	68.5	0.742
108	8	47.2	67.3	0.732
			Average C_m	0.726
131	24	62.2	111.1	0.616
132	24	66.9	108.5	0.584
133	24	--	103.9	0.673
134	24	50.1	95.8	0.521
			Average C_m	0.599

APPENDIX C

PHOTOELASTIC EVALUATION OF PLASTIC ZONES

In order to determine the size and shape of the plastic zones in representative specimens, it was decided to use a photoelastic coating bonded to the specimens by an adhesive. This appendix provides some discussion of the theoretical basis for the plastic-zone determinations, details of techniques, and the results of a limited series of tests.

Theoretical Basis for Photoelastic Measurements

To apply a theoretical criterion for yield, such as the Tresca (or maximum shear stress) or the von Mises (or distortion energy) criteria, one must measure all three components of principal strain (ϵ_1, ϵ_2, ϵ_3). Here ϵ_1 and ϵ_2 are the in-plane components and the third principal strain, ϵ_3, represents the thickness change. An essential problem arises in application of the photoelastic technique since only the principal strain difference, $\epsilon_1 - \epsilon_2$, is measured. Only an approximate indication of yield can be obtained, and the accuracy of the method was therefore evaluated.

Dixon* states that the material inside the photoelastic fringe

$$\epsilon_1 - \epsilon_2 = \frac{Y}{E}(1 + \nu)$$

is plastic according to the Tresca criterion, where Y is the material yield strength, E is Young's modulus, and ν is Poisson's ratio. However, material outside the fringe may or may not be plastic. On the other hand, thickness change measurements indicate yield of material inside the contour

$$\epsilon_3 = \frac{2\nu 2}{1 - \nu},$$

and material outside may or may not be plastic.

Figure C-1 is based on calculations of the types of strain fields associated with crack tips and shows the merits of the two methods. The plots are based on data from the finite element calculations with the "true" plastic zone as determined by the von Mises yield criterion of the computer program. Distributions of the strain difference and thickness changes were calculated and these gave rise to the two dashed-line zone shapes. The strain-difference zone is in quite good agreement with the "true" calculated zone. The slight discrepancy is believed due primarily to the inherent difference between the Tresca and von Mises yield criteria. The zone indicated by thickness change is considerably smaller than the "true" zone, and only in a very small region on the crack plane does it give a larger zone than that given by the strain-difference technique.

*Dixon, J. R., and Strannigan, J. S., "Effect of Plastic Deformation on the Strain Distribution Around Cracks in Sheet Materials", J. Mech. Eng. Sci., 6, pp 132-136 (1964).

It is concluded that the strain-difference fringes as measured by a photoelastic-coating technique can give a reliable measure of the plastic zone at the end of a crack, and the contour

$$\epsilon_1 - \epsilon_2 = \frac{Y}{E}(1 + \nu) ,$$

can be used to define the boundary between the elastic and plastic regions.

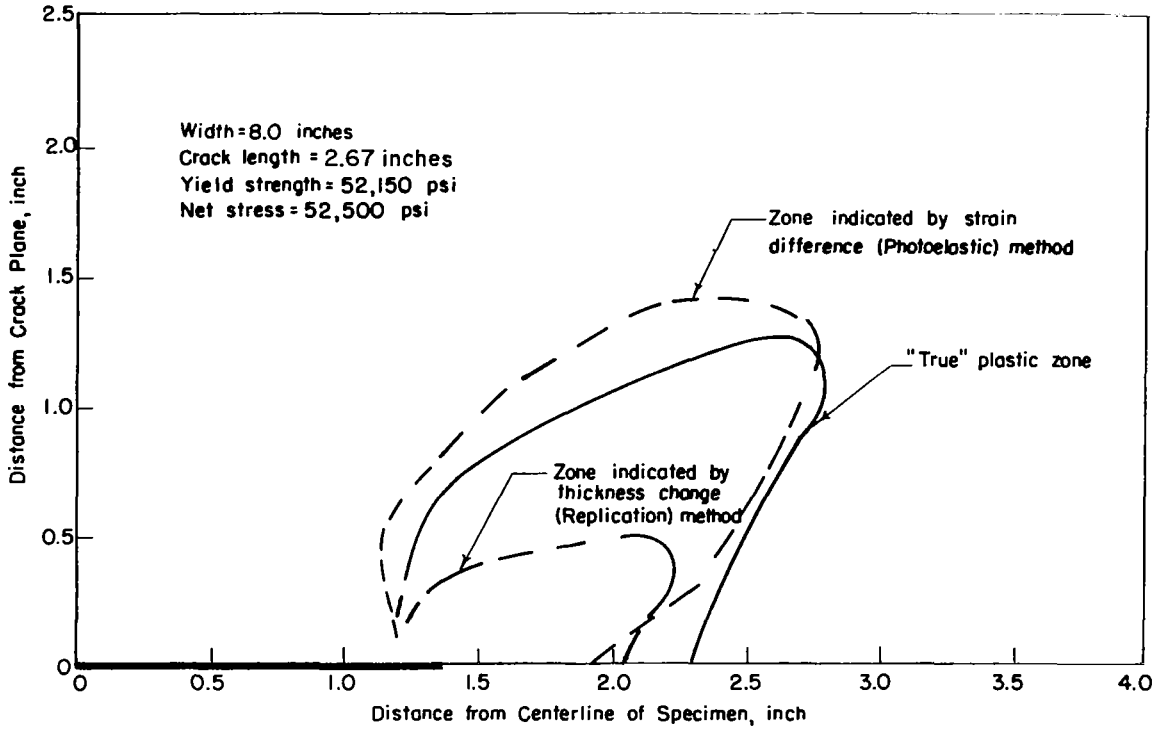

FIGURE C-1. COMPARISON OF COMPUTED PLASTIC ZONE WITH CORRESPONDING ZONES MEASURABLE BY STRAIN-DIFFERENCE AND THICKNESS-CHANGE METHODS

Photoelastic Tests and Results

In the photoelastic surface-coating technique, a layer of suitably birefringent material is cemented to the surface of the specimen. On loading the specimen, surface strains produced in the specimen are reproduced through the birefringent layer. Polarized light passed through the layer is reflected from the specimen surface and back through the layer to produce a visual fringe pattern. The pattern then can be analyzed in the normal photoelastic manner.

This procedure was essentially followed for Specimens 97, 98, 99, and 126. A birefringent coating, 20 mils thick, having a strain sensitivity of 3790 microinches per inch per fringe was cemented to each specimen with an epoxy adhesive. An adhesive line of 6 to 8 mils was used.

The coating was selected for a number of reasons. Mainly, it has the highest sensitivity, K = 0.15, of any commercial photoelastic plastic coupled with a relatively high maximum elongation of 10 percent. Thus, the coating is quite suited to determination of post-yield strains. The adhesive was selected for its properties of combined high strength and modulus characteristics with high elongation which makes it suitable for post-yield investigations. The thickness of the coating was selected to give approximately two fringe orders at yield.

In the coating technique, the strain difference in the plane of the object studied is related to the photoelastic and other properties of this coating and light by the equation

$$\epsilon_1 - \epsilon_2 = N\lambda/2tk = Nf;\ f = \lambda/2tk\ ,$$

where

$\epsilon_1 - \epsilon_2$ = principal strain difference, microinches/inch

N = fringe order

t = coating thickness, inch

λ = wavelength of light extinguished, microinches (22.7 microinches)

K = photoelastic sensitivity, per fringe

f = coating sensitivity, microinches per inch per fringe.

From this equation, it is possible to determine the thickness of material required to produce a given fringe order at a given strain difference. It was calculated from the von Mises yield criteria that the material in question would yield at a minimum strain difference of approximately 6550 microinches. Entering this value for the strain difference in the above equation along with K = 0.15 and N = 2, it was determined that a thickness of 0.023 inch was required. Commercially available thicknesses are 0.010, 0.020, 0.040, 0.080, and 0.120; thus, a sheet with a thickness of t = 0.020 inch was selected having a sensitivity of f = 3790 microinches per inch per fringe.

The coating covered approximately a square area, spaced equally above and below the crack and probable crack path on one-half of one side of the specimen. Over this coating was placed a combined polarizing and quarter-wave sheet producing, in essence, a circular dark-field polariscope. Fringe patterns as a function of load (the load was applied at a fixed rate as a function of time) were recorded by means of a 16-mm movie camera from load initiation to specimen fracture. Timing pips on the film edge were used for load reference. Various frames from each film then were enlarged by a microfilm reader and the fringe patterns were traced. In general, the frames selected consisted of those at designated pip points, usually one pip before estimated initiation of slow crack growth, at slow growth, and two or three frames after initiation of slow growth. The final frame selected was always one of the last two frames before complete fracture of the specimen.

Table C-1 contains some of the details concerning the specimen sizes and loads at which each fringe-strain pattern was traced. Figures C-2 through C-5 show the tracings of the integral fringe patterns from the indicated frames for each test specimen. These strain fields accurately represent the planar strain fields that are present in the specimens during testing.

TABLE C-1. SPECIMEN DETAILS AND STRESS PATTERN LOADS

Specimen No.	Thickness	Width	Aspect Ratio	Pip No.	Load	Figure No.
97	0.125	8.0	0.3	7	23,300	C-1a
				8*	26,200	b
				9	29,400	c
				10	33,000	d
				Failed	34,300	e
98	0.500	8.0	0.3	5	52,000	C-2a
				6*	66,000	b
				9	101,000	c
				10	113,700	d
				Failed	122,500	e
99	0.051	8.0	0.3	5	6,400	C-3a
				6*	7,950	b
				7	9,050	c
				8	10,500	d
				9	12,100	e
				Failed	12,790	f
126	0.123	24.0	0.1	18*	94,500	C-4a
				21	111,850	b
				23	123,000	c
				24	129,000	d
				25 Failed	132,000	e

*Estimated initiation of slow crack growth.

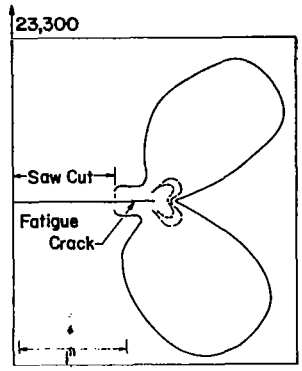

a. 23, 300 Pounds

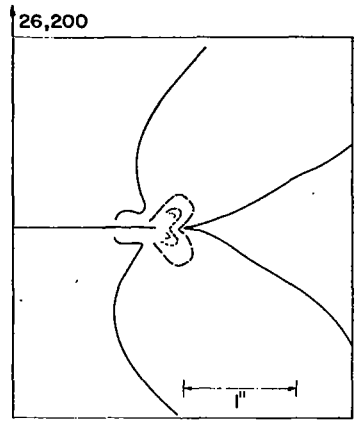

b. 26, 200 Pounds

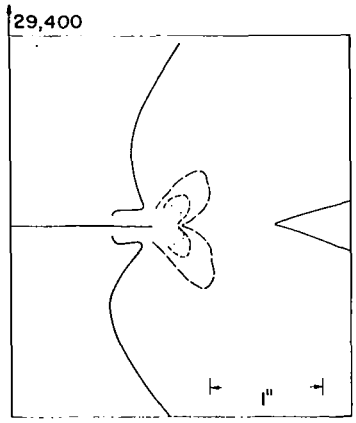

c. 29, 400 Pounds

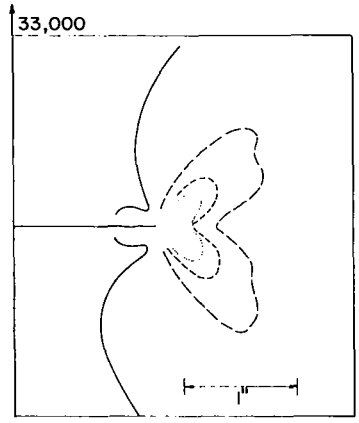

d. 33, 000 Pounds

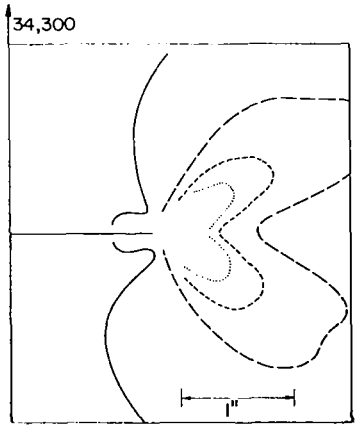

e. 34, 300 Pounds

FRINGE ORDER	$\epsilon_1 - \epsilon_2$ in./in.
1 ———	0.00379
2 — — —	0.00758
3 - - - -	0.01137
4	0.01516

FIGURE C-2. FRINGE PATTERNS FOR SPECIMEN 97

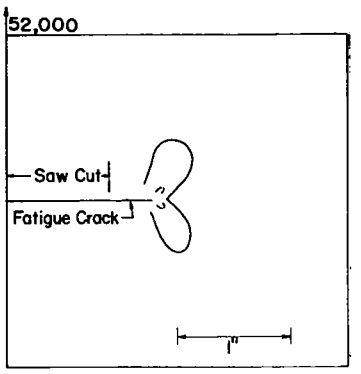

a. 52,000 Pounds

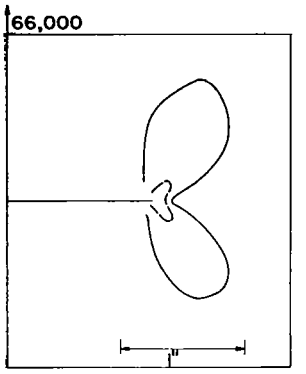

b. 66,000 Pounds

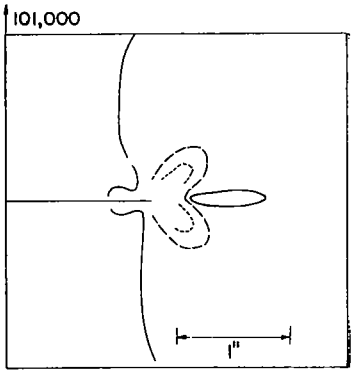

c. 101,000 Pounds

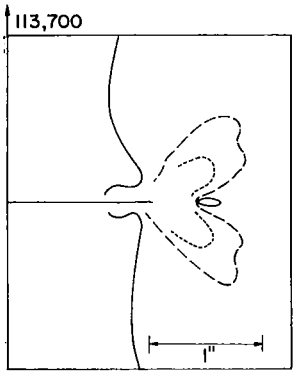

d. 113,700 Pounds

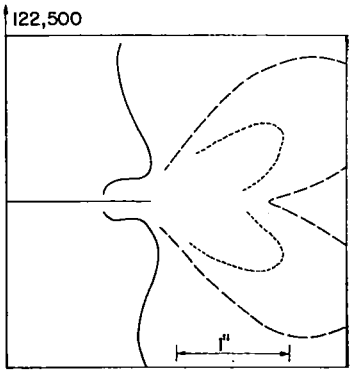

e. 122,500 Pounds

FRINGE ORDER	$\epsilon_1 - \epsilon_2$ in./in.
1 ———	0.00379
2 – – – –	0.00758
3 ———	0.01137

FIGURE C-3. FRINGE PATTERNS FOR SPECIMEN 98

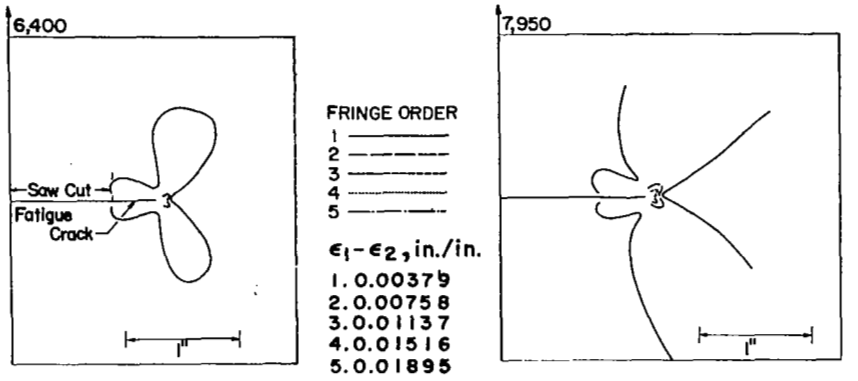

a. 6,400 Pounds

b. 7,950 Pounds

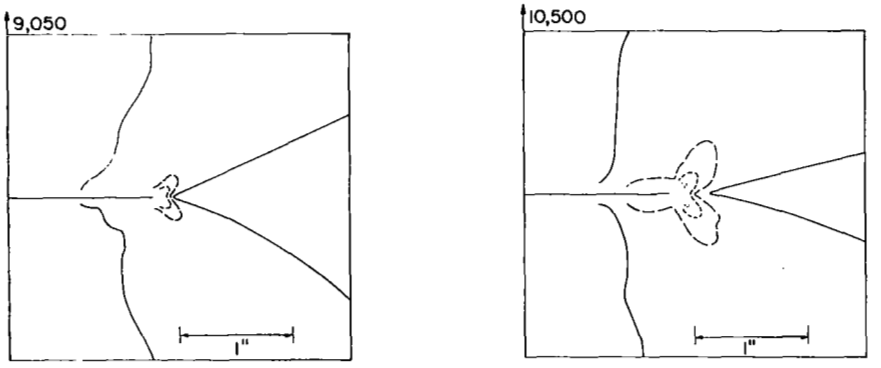

c. 9,050 Pounds

d. 10,500 Pounds

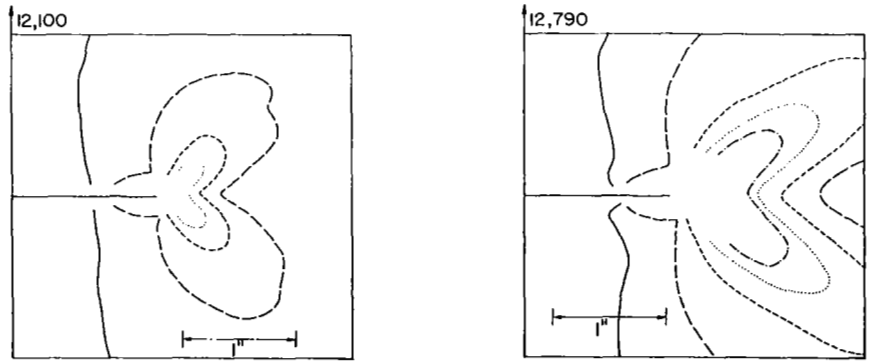

e. 12,100 Pounds

f. 12,790 Pounds

FIGURE C-4. FRINGE PATTERNS FOR SPECIMEN 99

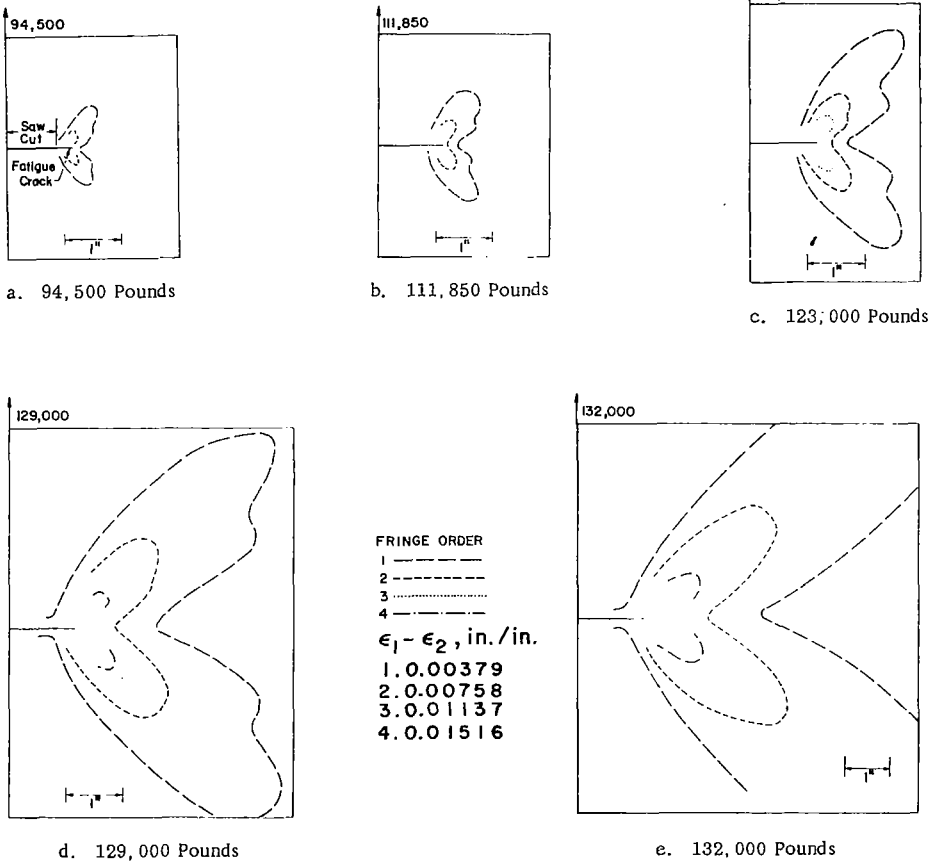

a. 94,500 Pounds

b. 111,850 Pounds

c. 123,000 Pounds

d. 129,000 Pounds

e. 132,000 Pounds

FIGURE C-5. FRINGE PATTERNS FOR SPECIMEN 126

NASA-Langley, 1970 —— 17 CR-1678